สัญญาเลขที่ R2559C055

รายงานวิจัยฉบับสมบูรณ์

ผลของปริมาณ FeO ที่ต่อโครงสร้างเฟส โครงสร้างจุลภาคและสมบัติทางไฟฟ้าของเซรามิก NKLNST ที่เตรียมด้วยเทคนิคการเผาไหม้

Effect of FeO content on phase formation, microstructure and electrical properties of NKLNST ceramics prepared via combustion technique

อ.ศุภรพรรณ ชูถิ่น
ผศ.ดร.ธีระชัย บงการณ์
ภาควิชาฟิสิกส์ คณะวิทยาศาสตร์ มหาวิทยาลัยนเรศวร

สนับสนุนโดยกองทุนวิจัยมหาวิทยาลัยนเรศวร

กิตติกรรมประกาศ

งานวิจัยนี้ได้รับการสนับสนุนงบประมาณจากกองทุนวิจัยมหาวิทยาลัยนเรศวร ผู้วิจัยและคณะขอขอบพระคุณ ณ โอกาสนี้

ขอขอบคุณเจ้าหน้าที่ภาควิชาฟิสิกส์ คณะวิทยาศาสตร์ มหาวิทยาลัยนเรศวร ทุกท่านซึ่งอำนวยความสะดวกเกี่ยวกับอุปกรณ์เครื่องมือต่างๆ

ขอขอบคุณ Science Lab Center คณะวิทยาศาสตร์ มหาวิทยาลัยนเรศวร ที่สนับสนุนเครื่องมือและอุปกรณ์ในการทำวิจัย

อ.ศุภรพรรณ ชูถิ่น และคณะ

หัวข้อวิจัย ผลของปริมาณ FeO ที่ต่อโครงสร้างเฟส โครงสร้างจุลภาคและสมบัติทางไฟฟ้าของเซรามิก NKLNST ที่เตรียมด้วยเทคนิคการเผาไหม้

นักวิจัย อ.ศุภรพรรณ ชูถิ่น
ผศ.ดร.ธีระชัย บงการณ์

บทคัดย่อ

เซรามิกเพียโซอิเล็กทริกปราศจากตะกั่ว $(K_{0.44}Na_{0.52}Li_{0.04})(Nb_{0.84}Ta_{0.10}Sb_{0.06})O_3$ (KNLNTS) เจือด้วย Fe_2O_3 ที่องค์ประกอบ 0 และ 1.0 wt% เตรียมด้วยวิธีการเผาไหม้โดยใช้ไกลซีนเป็นเชื้อเพลิง การเจือ Fe_2O_3 มีผลต่อการก่อเกิดเฟส ลักษณะสัณฐาน ความหนาแน่น สมบัติทางไฟฟ้าและแม่เหล็ก โครงสร้างผลึกของเซรามิกที่เจือ $Fe_2O_3 \leq 0.6$ wt% แสดงเฟสเพอรอฟสไกต์บริสุทธิ์ ในขณะที่ $Fe_2O_3 > 0.6$ wt% พบเฟสแปลกปลอม $FeNbO_4$ และ $FeTaO_4$ การเกิดเฟสเปลี่ยนจากเฟสออโทโกนอลเป็นเฟสออโทรอมบิกและคิวบิกมากขึ้นเมื่อเจือ Fe_2O_3 เพิ่มขึ้นจาก 0 เป็น 1.0 wt% โครงสร้างจุลภาคแสดงรูปร่างของเกรนคมชัดที่มีลักษณะเป็นสี่เหลี่ยมในทุกตัวอย่าง ค่าเฉลี่ยของขนาดเกรนและความหนาแน่นของเซรามิกเพิ่มขึ้นจาก 1.52 เป็น 2.10 μm และ 4.42 to 4.65 g/cm^3 เมื่อเพิ่มปริมาณ Fe_2O_3 จาก 0 เป็น 0.6 wt% ค่าไดอิเล็กทริกสูงสุด (ε_r ที่ T_r = 2782 และ ε_m ที่ T_C = 7520), ค่าเฟร์โรอิเล็กทริก (P_r = 27.9 μC/cm^2 และ E_c= 9.9 kV/cm) และค่าเพียโซอิเล็กทริกสูงสุด (d_{33} = 311 pC/N) พบที่ตัวอย่างเจือ Fe_2O_3 = 0.6 wt% ซึ่งตัวอย่างนี้แสดงพฤติกรรมเฟร์โรแมกนีติก (M_r = 0.015 emu/g และ H_c = 143 Oe) การเจือ Fe_2O_3 ที่ปริมาณที่เหมาะสมและวิธีการเตรียมด้วยวิธีการเผาไหม้เป็นวิธีการใหม่ที่สามารถปรับปรุงค่าความหนาแน่น โครงสร้างจุลภาค สมบัติเพียโซอิเล็กทริก สมบัติเฟร์โรอิเล็กทริกและสมบัติเฟร์โรแมกนีติก

Research Topic: Effect of FeO content on phase formation, microstructure and electrical properties of NKLNST ceramics prepared via combustion technique

Researcher: Ms. Supornpun Chootin
Assist. Prof. Dr.Theerachai Bongkarn

ABSTRACT

Lead-free piezoelectric $(K_{0.44}Na_{0.52}Li_{0.04})(Nb_{0.84}Ta_{0.10}Sb_{0.06})O_3$ (KNLNTS) ceramics doped with Fe_2O_3 at compositions between 0 and 1.0 wt% were prepared by the solid state combustion method with glycine used as the fuel. The effect of Fe_2O_3 doping on the phase formation, morphology, density, electric and magnetic properties was investigated. The crystal structure of the ceramics doped with $Fe_2O_3 \leq$ 0.6 wt% exhibited a pure perovskite phase, while the secondary phases of $FeNbO_4$ and $FeTaO_4$ were detected in the ceramics doped with Fe_2O_3>0.6 wt%. The phase formation changed from orthogonal phase to the dominated orthorhombic phase and cubic phase when Fe_2O_3 doping increased from 0 to 1.0 wt%. The microstructure exhibited a rectangular shape grain in all samples. The average grain size and the density of the ceramics increased from 1.52 to 2.10 μm and 4.42 to 4.65 g/cm^3 by increasing Fe_2O_3 content from 0 to 0.6 wt% then dropping in a value with further Fe_2O_3 doping. The highest dielectric constant (ε_r at T_r = 2782 and ε_m at T_C = 7520), excellent ferroelectric properties (P_r = 27.9 μC/cm^2 and E_c= 9.9 kV/cm) and the highest d_{33} (311 pC/N) were obtained from the sample doped with 0.6 wt% Fe_2O_3. This sample exhibited ferromagnetic behavior with M_r and H_c of 0.015 emu/g and 143 Oe, respectively. The dopant of Fe_2O_3 at appropriate amount and the solid state combustion technique are a new alternative for increment and improvement of densification, microstructure, piezoelectric, ferroelectric and ferromagnetic properties.

CHAPTER I

INTRODUCTION

Rationale for the study and statement of the problem

$K_{0.5}Na_{0.5}NbO_3$ (KNN) solid solution is one of the best-known lead-free piezoelectric compounds and has been widely studied. KNN exhibits perovskite structure at room temperature, possesses a good dielectric constant (ε') and has high Curie temperature. However, pure KNN solid solution exhibits relatively low piezoelectric coefficient (d_{33}=~80pC/N) and poor remnant polarization (P_r ~11 μC/cm^2) [1-3]. Moreover, there is difficulty in obtaining high densification when it is synthesized by conventional sintering [4]. Improved KNN-based ceramics have been developed by adding $LiTaO_3$ [5], $LiSbO_3$ [6], $LiNbO_3$ [7], $CaTiO_3$ [8], and $SrTiO_3$ [9]. This improved the sinterability, piezoelectric and ferroelectric properties of these ceramics. The modified KNN ceramics by $LiTaO_3$ adding at 5 mol% exhibited high d_{33} value of 200 pC/N as reported by Y. GaO et al. [10]. The high d_{33} (171 pC/N) and good remnant polarization (P_r ~18 μC/cm^2) of KNN ceramics were obtained from adding $LiSbO_3$ at 6 mol% [11]. M. Jiang et al. [12] reported the d_{33} value of $(K_{0.44}Na_{0.52}Li_{0.04})(Nb_{0.84}Ta_{0.10}Sb_{0.06})O_3$ (KNLNTS) ceramics fabricated by conventional technique is about 92 pC/N. Recently, Safari et al. [13] synthesized KNLNTS ceramics by mixed-oxide route using sintering temperature of 1150°C for 1 h. The maximum d_{33} value (≅300 pC/N) and good ferroelectric properties (P_r ~21.1 μC/cm^2 and E_c~8.2 kV/cm measured at 30 kV/cm) were obtained by sample prepared under special conditions which are as follows; (i) heat treatment of raw materials at

220°C for 24 h, (ii) powder process performed in glove box with Ar gas flowing and (iii) samples were sintered in high O_2 atmosphere (360 cm^3/min). In addition, Saito et al. [14] reported that a large piezoelectric coefficient (d_{33}≅400 pC/N) was obtained by texture ceramic of KNLNTS fabricated by the reactive templated grain growth (RTGG) method.

Nowadays, H.N. Ji and coworkers [15] reported an alternate way to improved electrical properties and densification in KNN-based ferroelectric perovskite ceramics. They doped FeO into $0.95(K_{0.52}Na_{0.48})NbO_3$-$0.05LiSbO_3$ (KNN-LS) ceramics prepared by conventional solid sintering. This system demonstrated a d_{33} value (311 pC/N), a dielectric constant (~9000) and relative density (97%) at 1.0 mol% FeO doping, which is higher than pure KNN-LS ceramics. R. Zuo et.al. [16] found that the $(K_{0.5}Na_{0.5})_{0.96}Li_{0.04}Nb_{0.86}Ta_{0.1}Sb_{0.04}O_3$ ceramics doped at 0.25 mol% of Fe_2O_3 synthesized via solid state reaction can exhibit high density and d_{33} of 98% and 241 pC/N, respectively. After that, Y.P. Ok et al. [17] fabricated $(K_{0.38}Na_{0.58}Li_{0.04})(Nb_{0.86}Ta_{0.10}Sb_{0.04})O_3$ (KNL-NTS) ceramic by doping of a small amount Fe_2O_3 (0, 0.3, 0.5, and 1 mol%) via conventional solid state reaction technique. The results concluded that the addition of Fe_2O_3 at amount 0.3 mol% can enhance the density (91.9%) and increase the piezoelectric constant d_{33} (257 pC/N). They also reported that the dopants of FeO and Fe_2O_3 could promote the grain size of KNN-based ceramics [15-17]. Moreover, many researchers have been systematically studied the structural, magnetic, electrical and magnetroelectric behaviors of Fe^{3+} ion doped in ferroelectric perovskite ceramics ($BaTiO_3$, $SrTiO_3$, and $KTaO_3$) and these compounds exhibited a probable magnetoelectric responses at room temperature [18-20]. So, doping of Fe_2O_3 in the right proportion is an effective method of improving the

densification and the electrical properties and produces ferromagnetism in ferroelectric perovskite ceramics. Accordingly, the concept for improving the KNLNTS solid solution with Fe_2O_3 doping at concentrations between 0 and 1.0 wt% in order to enhance the density, ferroelectric and ferromagnetic properties is of great interest and a challenge.

It is well known that the fabrication of piezoelectric ceramics via conventional solid state reaction method is performed at high temperature which conducts volatility some of raw materials and gains large agglomerated powders. These always make obtaining impurities phase, low density and low electrical properties ceramics [12, 14, 21]. Recently, T. Bongkarn and coworkers [22-27] successfully fabricated high quality lead-free piezoelectric ceramics of single, binary and ternary systems by the solid state combustion technique, for example KNN-LS-BS [22], BNKLLT [23], BCTZ [24], BNKLT-BZT [25], BNKTNb-LSb [26], BNT-BKT-KNN-BCTZ [27]. This technique was modified from a solid-state reaction technique. The technical feature of the combustion technique is the released energy obtained from the decomposition reaction of the fuel, which speeds up the chemical reaction of the raw materials. The liquid phase caused from the melting of the fuel creates easy diffusion of the raw materials [21-28]. The powders obtained have a higher purity, are more homogenous, have a finer particle size, require lower firing temperature and have a shorter dwell time than powder synthesyzed via the conventional method.

From a review of the literature, it was observed that the preparation of the KNLNTS with Fe_2O_3 doping by the solid state combustion technique had not been investigated. Hence, in this paper, we synthesized the KNLNTS lead-free piezoelectric ceramics with Fe_2O_3 doping between 0 and 1.0 wt% by the solid state

combustion technique and investigated the effect of Fe_2O_3 content on the phase formation, morphology, dielectric, ferroelectric, piezoelectric and ferromagnetic properties. The optimum amount of Fe_2O_3 doping for the increment of density, electric and magnetic properties was also evaluated.

Objectives of this research

The objectives of this research are as follow:

1. To prepare KNLNTS with Fe_2O_3 doping ceramics using the solid state combustion technique.

2. To investigated the optimum calcination and sintering conditions of KNLNTS with Fe_2O_3 doping ceramics by the solid state combustion technique.

3. To study the effect of calcination and sintering temperatures on phase formation, microstructure , electrical and magnetic properties of KNLNTS with Fe_2O_3 doping ceramics by the solid state combustion technique.

CHAPTER II

THEORY AND LITERATURE

This chapter contains details on the brief description of necessary concepts of the perovskite ferroelectrics. In addition, the relevant literatures on processing and characteristics of both powders and ceramics are reviewed with attention paid on their properties.

Perovskite Structure

Since the ferroelectric properties of barium titanate were reported by Von Hippel in 1945, ABO_3 compound with the perovskite structure have been studied extensively. These studies have resulted in the discovery of many new ferroelectric and piezoelectric materials. Most of the literatures on perovskite-type compounds have concentrated on these properties.

Perovskite structure is a crystal structure of a mineral perovskite calcium titanate ($CaTiO_3$) which was discovered by Count Lev Aleksevich von Perovski [49]. This structure is adopted by many oxides that the general chemical formula of ABO_3. The general crystal structure is a primitive cube which the A represents a cation with larger ionic radius in the corner, B represents a cation with a smaller ionic radius in the middle of the cube and O is oxygen in the centre of the face edges. Figure 1 shows a cubic perovskite structure unit cell (a) and three-dimensional network of BO_6 octahedra (b). The sites are occupied by Ba^{2+}, Pb^{2+}, K^+ or Na^+ ions, and B sites by Ti^{4+}, Zr^{4+}, Nb^{5+} or Ta^{5+} ions. Some examples of perovskite-type ceramic compounds are lead titanate ($PbTiO_3$), barium titanate ($BaTiO_3$), bismuth sodium titanate ($Bi_xNa_{1-x}TiO_3$), potassium niobate ($KNbO_3$), etc. The perovskite structure can tolerate a wide range of compositional variation. Thus, its properties are differed behavior [48, 50, 51].

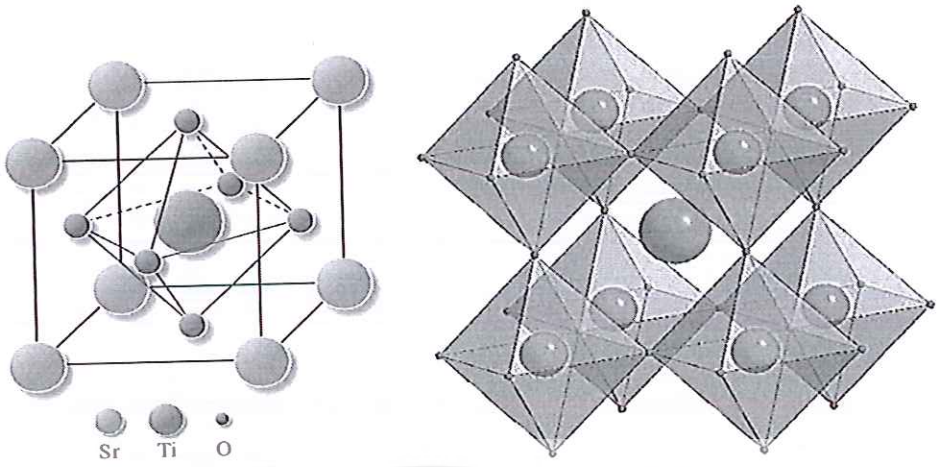

Figure 1 (a) A cubic $SrTiO_3$perovskite-type unit cell and (b) three-dimensional network of BO_6 octahedra [49]

Piezoelectricity

Piezoelectricity was discovered in 1880 by Jacques and Pierre Curie during their systematic study of the effect of pressure on the generation of a electrical charge by crystals such as quartz, zincblend, and tourmaline [51]. The name "piezo" is derived from the Greek, meaning "to press", hence piezoelectricity is the generation of electricity as a result of mechanical pressure. Many piezoelectric materials are not ferroelectric but all ferroelectrics are piezoelectric. Two effects are operative in piezoelectricity. The direct effect is identified with the phenomenon whereby an electrical charge (polarization) is generated from mechanical stress, whereas the converse effect is associated with the mechanical movement generated by the application of an electrical field. Both of these effects are illustrated in Figure 2.

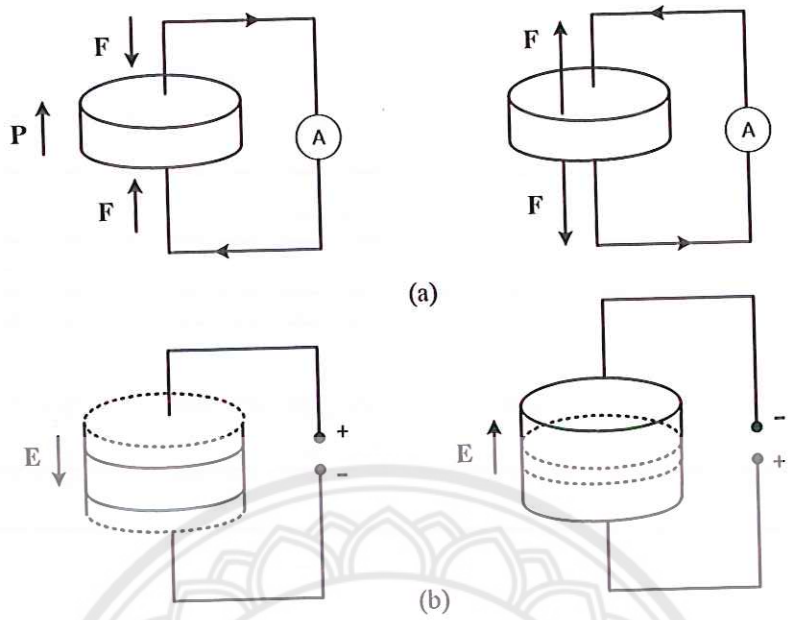

Figure 2 Piezoelectric effects in ferroelectric ceramics (a) direct effect (b) converse effect [51]

The basic equations that describe these two effects in regard to electric and elastic properties are

$$D = dT + \varepsilon^T E \quad (1)$$

$$S = s^E T + dE \quad (2)$$

Where D is the dielectric displacement (consider it equal to polarization), T the stress, E the electric field, S the strain, d a piezoelectric coefficient, s the material compliance (inverse of modulus of elasticity), and ε the dielectric constant (permittivity). The subscripts indicate a quantity held constant: in the case of ε^T, the stress is held constant, which means that the piezoelectric element is mechanically unconstrained, and, in the case of s^E, the electric field is held constant, which means the electrodes on the element are shorted together.

Ferroelectrics

Ferroelectricity is a phenomenon which was discovered by Valasek in 1921 [52]. It has become customary to call ferroelectricity the phenomenon exhibited by these crystals and ferroelectric the crystal themselves. This is due to a formal similarity of the ferroelectric phenomenon with that of ferromagnetism. The similarity is mainly phenomenological. As ferromagnetic materials exhibit a spontaneous magnetization and hysteresis effects in the relationship between magnetization and magnetic field, ferroelectric crystals show a spontaneous electric polarization and hysteresis effects in the relation between the dielectric displacement and the electric field. This behavior is mostly observed in certain temperature regions below by transition temperature (Curie temperature) where those crystals above are this transition temperature are no longer ferroelectric.

The crystal symmetries of the paraelectric and ferroelectric phase are an important factor in displaying the ferroelectric behavior of the materials. The lattice structure described by the Bravais unit cell of the crystal governs the crystal symmetry. Though there are thousands of crystals in nature, they all can be grouped together into 230 microscopic symmetry types or space groups based on symmetry elements. It can be shown by the inspection of the 230 space groups that there are just 32 point groups. As shown in Figure 3, the 32 point groups can be further classified into (a) crystal having a center of symmetry and (b) crystals which do not possess a center of symmetry (noncentrosymmetric). There are 21 classes of noncentrosymmetric, a necessary condition for piezoelectricity to exist, and only 20 are piezoelectric. Among these 20 point groups, only 10 can display a spontaneous polarization, which is designated as pyroelectric. A subgroup of the spontaneous polarized pyroelectric is a category of materials known as ferroelectrics. Ferroelectrics are a special class of materials in which a permanent electric dipole can be reoriented between equilibrium states by the external electric field. Continuing Valasek's analogy between ferroelectric and ferromagnetic, the dependence of the polarization on an applied electric field can be seen by polarization versus electric field i.e. (P-E) hysteresis loop as shown in Figure 4. The hysteresis loop is typically observed using the simple circuit described by Sawyer-Tower [53]. One parameters obtained from the hysteresis loop measurement, the remnant polarization (P_r) is the crystal spontaneous

polarizes along one of the allowed direction without applied electric field. The field required to reverse the polarization is known as the coercive field (E_c).

Normal ferroelectric materials have a sharp phase transition which occurs at a specific temperature called the Curie temperature, T_c. The T_c is the temperature which the crystal structure transforms from the paraelectric state into the ferroelectric state and vice versa [48, 54, 55]. In the paraelectric state, the dielectric permittivity obeys the Curie-Weiss law.

$$\varepsilon_r = \frac{C}{T - T_0} \tag{3}$$

Where C is the Curie-Weiss constant, T is the temperature and T_0 is the Curie-Weiss temperature. The Curie temperature (T_c) and the Curie-Weiss temperature (T_0) should not be confused. The Curie temperature is the actual transformation temperature, but the Curie-Weiss temperature is found by extrapolating the plot of the Curie-Weiss law, as shown in Figure 5. The Curie temperature and Curie-Weiss temperature typically differ by only a small amount that depends on the type of phase formation the material undergoes. The Curie-Weiss temperature can be as much as ten degrees lower than the Curie temperature for first-order phase transformations and the two can be nearly equal for second-order phase transformations (first order phase transformations are those in which the first derivative of the free energy, with respect to temperature, is discontinuous; second order phase transitions are those in which the second derivative is discontinuous).

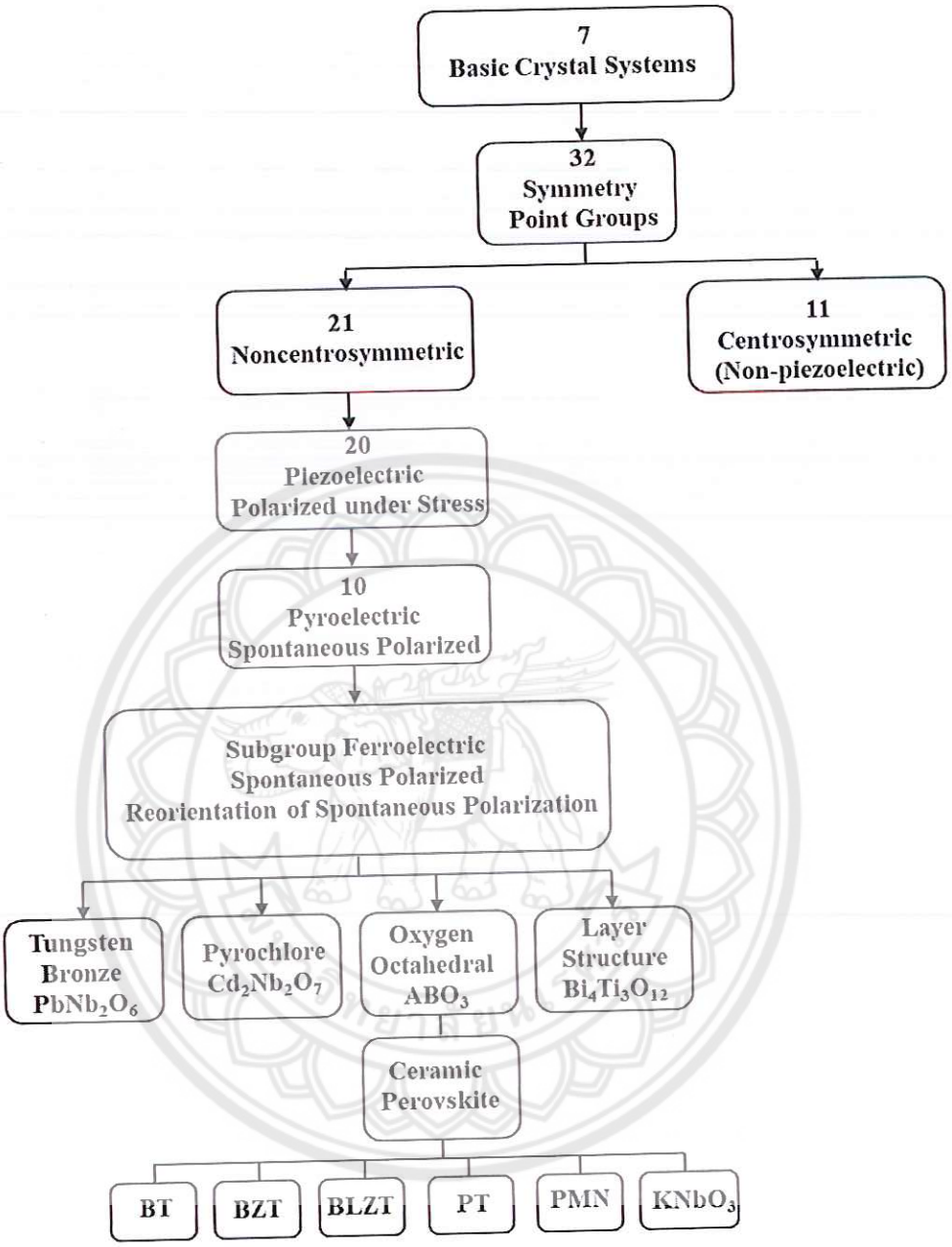

Figure 3 Interrelationship of piezoelectric and subgroups on the basis of symmetry [50]

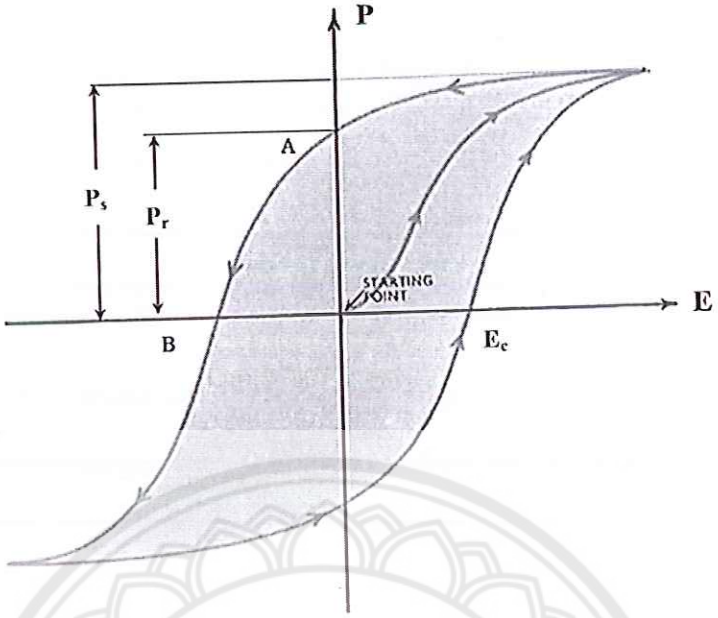

Figure 4 A ferroelectric hysteresis loop [56]

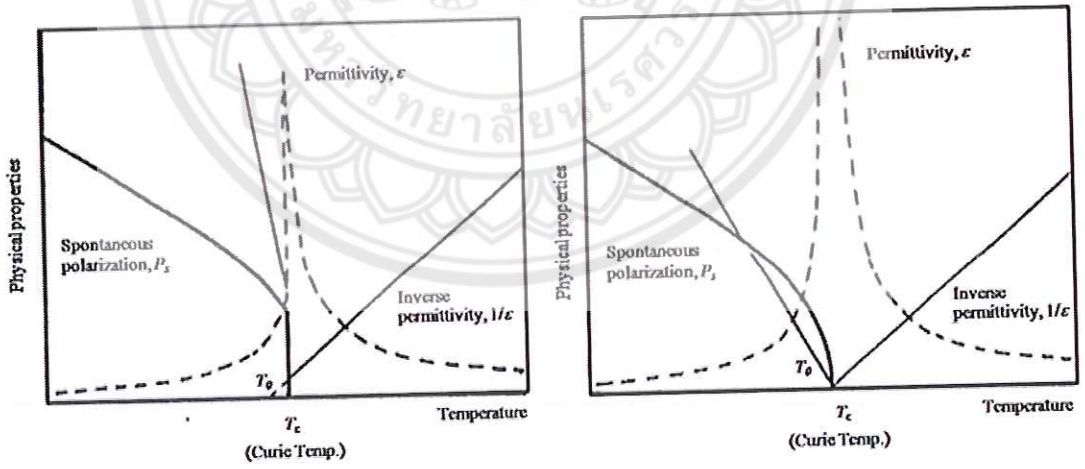

Figure 5 Phase transition in a ferroelectric (a) first order and (b) second order [54]

Antiferroelectric

An antiferroelectric crystal is defined as a crystal whose structure can be considered as being composed of two sublattices polarized spontaneously in antiparallel directions and in which a ferroelectric phase can be induced by applying an electric field. Experimentally, the reversal of the spontaneous polarization in ferroelectrics is observed as a single hysteresis loop, and the induced phase transition in antiferroelectrics as a double hysteresis loop (Figure 6), when a low-frequency ac field of a suitable strength is applied [57].

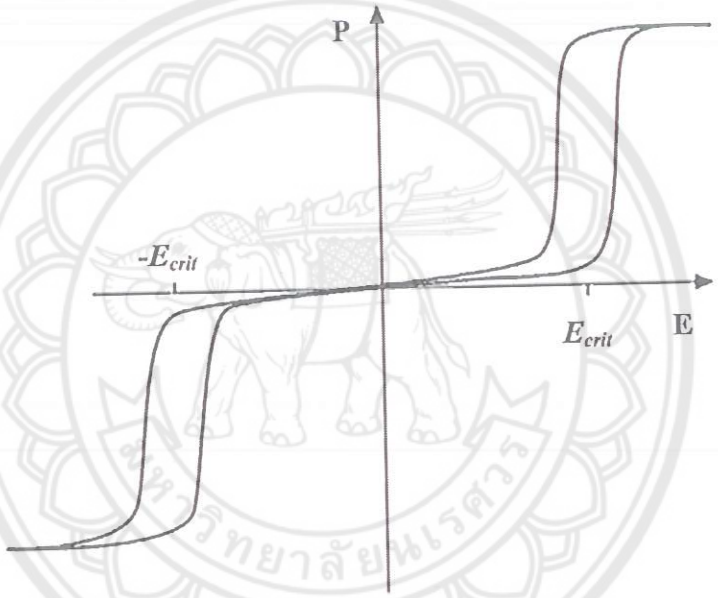

Figure 6 Antiferroelectric hysteresis loop [57]

Paraelectric

Paraelectricity is the ability of many materials (specifically ceramic crystals) to become polarized under an applied electric field. Unlike Ferroelectricity; this can happen even if there is no permanent electric dipole that exists in the material, and removal of the fields results in the polarization in the material returning to zero, as shown in Figure 7. The mechanisms which give rise to paraelectric behavior are the distortion of individual ions (displacement of the electron cloud from the nucleus) and the polarization of molecules or combinations of ions or defects. Paraelectricity occurs in crystal phases in which electric dipoles are unaligned (i.e. unordered

domains that are electrically charged) and thus have the potential to align in an external electric field and strengthen it. In comparison to the ferroelectric phase, the domains are unordered and the internal field is weak. The $LiNbO_3$ crystal is ferroelectric below 1430 K, and above this temperature it turns to paraelectric phase. Other perovskites similarly exhibit paraelectricity at high temperatures [58].

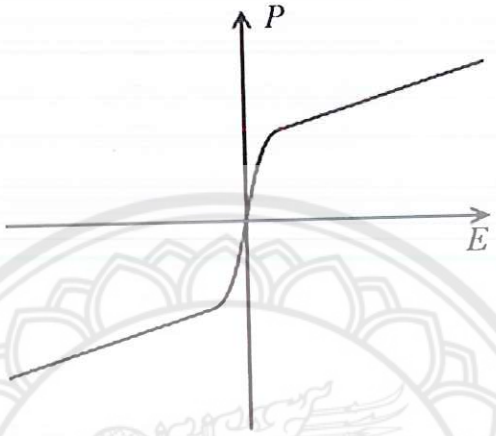

Figure 7 Paraelectric hysteresis loop [58]

Typical methods to synthesize ceramics

Solid-state reaction method

Solid-state reaction method is the most widely used method for the preparation of polycrystalline solids from a mixture of solid starting materials. This method involves chemical decomposition, where solid reactants are heated to produce a new solid and normally use simple oxides powders such as carbonates, hydroxides, nitrates, sulfates, acetates, oxalates, alkoxides and other metal salts for preparation. The solids do not react together at room temperature over normal time scales and it is necessary to heat them to much higher temperatures, often to 1000 to 1500 °C in order for the reaction to occur at an appreciable rate. An example of reaction between barium carbonate and titanium oxide at high temperature produce barium titanate by using solid-state reaction method.

$$BaCO_3(s) + TiO_2(s) \text{ -- (~1200 °C) -----> } BaTiO_3(s) + CO_2(g) \quad (4)$$

Solid-state reactions generally have an advantage in terms of production cost. However, it is commonly understood that the conventional solid state method requires compulsory grinding of different oxide mixtures for long periods of time as well as sintering. In addition, the synthesized component distributions are not homogeneous and particle sizes are relatively large [59, 60].

Sol-gel processing

Sol-gel process is a method for producing solid materials from small moleculesin a solution (sols) agglomerate and under controlled conditions eventually link together to form a coherent network (gel). The method is used for many applications in synthesis of novel materials. The advantages of the sol-gel process in general are high purity, homogeneity and low temperature. For a lower temperature process, there is a reduced loss of volatile components are thus the process is more environmental friendly. In addition, some materials that cannot be made by conventional means because of thermal and thermodynamically instability can be made by this process. However, the disadvantages are also real. The starting materials can be fairly expensive [61, 62].

Co-precipitation method

Co-precipitation (CPT) is the carrying down by a precipitate of substances normally soluble under the conditions employed. This method proceeds in two stages. First stage, the impurity is trapped either on the surface or inside the growing particles. If the growing particles have a crystal structure, then the impurity will become localized at regions of the solid phase with a perfect structure. During rapid precipitation, the growing particles will trap non-equilibrium impurities, which are usually in homogeneously distributed through the volume of the solid phase. In the second stage, the concentration of defects within the precipitate decrease and the particles are flocculated. Impurities trapped during the first stage return either partially or completely to the medium. The concentration of impurities in the solid phase becomes equalized. The crystals acquire an equilibrium composition that depends only on the composition and temperature of medium [61, 62].

Combustion method

Combustion method is the method based on the principle that once a reaction is initiated under heating, an exothermic reaction occurs from the oxidation-reduction reaction between reaction materials and fuel. It has emerged as an important technique for the synthesis and processing of advanced ceramics, which involves a self-sustained reaction. The advantages of this technique include inexpensive raw materials, simple and fast preparation process, fine powders with high homogeneity and low firing temperature and shorter dwell time [63, 64, 65]. The advantages of this method over other combustion methods are: firstly, being a solution process, it has control over the homogeneity and stoichiometry of the products; secondly, it is possible to incorporate desired impurity ions in oxide hosts and prepare industrially useful materials; thirdly, the process is simple and fast. Moreover, in fact, the reaction mechanism of this method is very complex due to there are several parameters influencing the reaction such as the type of fuel, fuel-oxidizer ratio, etc [66].

The fuel that used in combustion method was commonly an organic compound. Generally, a good fuel should reacted nonviolent, produce nontoxic gases, also acts as a chelating material for metal cations. It serve two purposes; first for the source of C and H which on combustion form CO_2 and H_2O and liberate heat and second for forming complexes with the metal ions facilitating homogeneous mixing of cations in solution. The nature of fuel and its amount are some of the important process parameter that influencing on the powder characteristics like a crystallite size, surface area nature of agglomeration, etc. The several fuels were used in the combustion method, e.g., urea, glycine, citric acid, alanine, carbohydrazide, poly acrylic acid, oxalic acid, acetyl acetone, metal acetate, hydrazine. Thus, the selection of an appropriate fuel is very important for the combustion system. Some properties of organic compounds used in combustion synthesis method are shown in Table 1. The commonly used fuels are; glycine, citric acid and urea. They were described as below;

1. Glycine

Glycine is one of the cheapest amino acids and is known to act as a complexing agent for a large amount of metallic ions. The glycine molecule has a carboxylic acid group located at one end of the chain and an amino group.

2. Citric acid

Citric acid is a weak organic acid that act as a convenient ligand which is inexpensive and is a more effective complexing agent for metal ions. The structure consists of three carboxyl groups and a hydroxyl group.

3. Urea

Urea is an attractive fuel for originating the formation of powders with crystallite sizes in the submicron/nanosized range and act as a complexing agent for metal ions because it contains two amino groups located at the extremes of its chemical structure.

Table 1 Some properties of organic compounds [67]

Properties	Organic component				
	Alanine	Glycine	Carbohydrazide	Urea	Citric acid
Structure formula	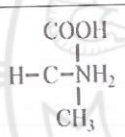	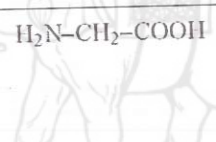	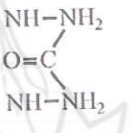	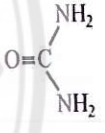	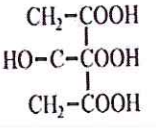
Molecular weight (g/mol)	80.1	90.1	75.1	60.1	192.1
Heat of combustion (kJ/g)	18.2	13.0	12.6	10.5	10.2
Decomposition temperature (°C)	314	262	153	135	175

The combustion method has been successfully used in the preparation of a large number of the ceramic oxide materials for a variety of applications which illustrated in Table 2. For example During the short span (> 15 years), many from the author's laboratory were becoming interested and attracted for producing fine grain size, crystalline and homogeneous ceramics at relatively low temperature and with reduced processing time. For example, Hwang, et al. [67] has investigated decomposition of the five fuels by acid or carbohydrazide. Some properties of five

fuels they select are shown in Table 1. The results of the thermal analysis show that there were different weight losses of organic fuels as presented in Figure 8. When using carbohydrazide as organic fuel, indicating that the chemical reaction took place very rapidly. But remaining weight is 22% of its original weight. While using glycine and alanine as organic fuels, the thermogravimetric of both demonstrated similar results. Their reactions are very fast and remaining weight lower than 10%. When using urea and citric acid as organic fuels, the chemical reaction was not rigorous when compared with glycine and alanine. Moreover, the crystal structure and microstructure of Ni-Zn ferrites prepared by combustion technique with various organic fuels was studies also. They result show that the pure phase of Ni-Zn was obtained while using glycine, alanine and corbohydrazide. While using urea and citric as organic fuels, the impurities phase was obtained existed in the diffraction pattern, as seen in Figure 9. The nanocrystalline sizes are ranging between 20.2 and 43.7 nm, as seen in Table 2. The results indicated that the ceramic synthesized by the combustion technique produced nanocrystalline sizes.

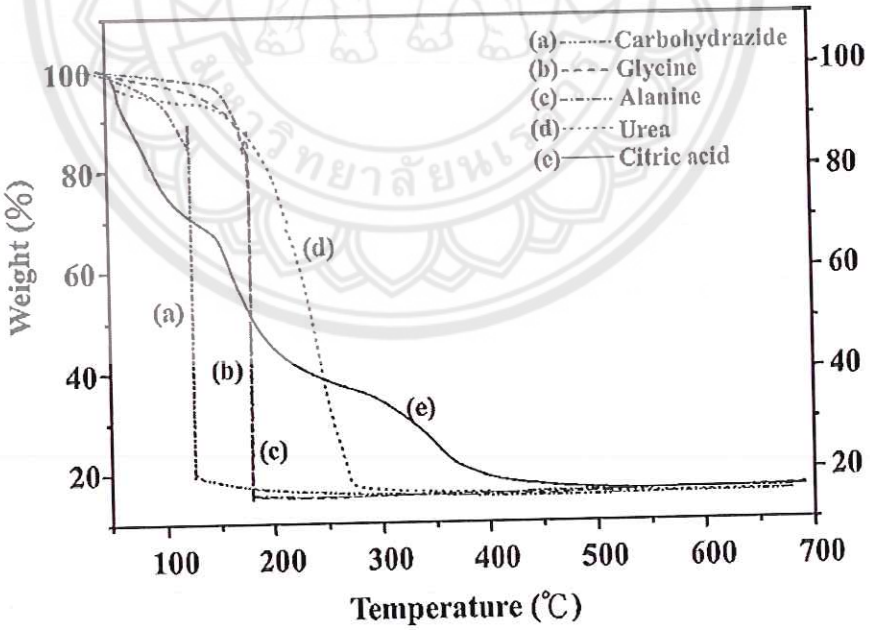

Figure 8 Thermogravimetric of various fuels [67]

Table 2 Oxide materials prepared by solution combustion method with the fuels

Material	Fuel	Particle size	Application
Al_2O_3	U	4 μm	Abrasive
Al_2O_3-ZrO_2	U	20-45 nm	Cutting tool
MAl_2O_4 (M=Mn and Zn)	AM+U/CH/ODH/GLY	15-28 nm	Catalytic support
$MgAl_2O_4$	U	13-20 nm	Structure material
CeO_2-ZrO_2	ODH	18 nm	Oxygen storage capacitor
	GLY	100 μm	Oxygen storage capacitor
$BaTiO_3$	GLY/CA	18-25 nm	Dielectric material
$Pb(Zr,Ti)O_3$	CA	~60 nm	Piezoelectric material
ZrO_2	GLY	23 nm	Oxygen sensor
$LiMn_2O_4$	PAA	30-60 nm	Lithium battery
$In_xGa_{1-x}O_3$	HY	54-160 nm	Optical coating for sensors
TiO_2	ODH	20 nm	Catalyst
	GLY	8-12 nm	Carcinogenic hexavalent chromium reduction
$LaBO_3$	U	55-75 nm (FESEM)	Decomposition of N_2O to N_2 and O_2
WO_3	GLY/U/thiourea	12-59 nm	Removal of organic dye from water
MgO	GLY	12-23 nm	Fluoride removal from drinking water

Note: U urea, AM metal acetate, CH carbohydrazides, ODH oxalidihidrazida, GLY glycine, CA citric acid, PAA poly acrylic acid, HY hydrazine. [68, 69, 70]

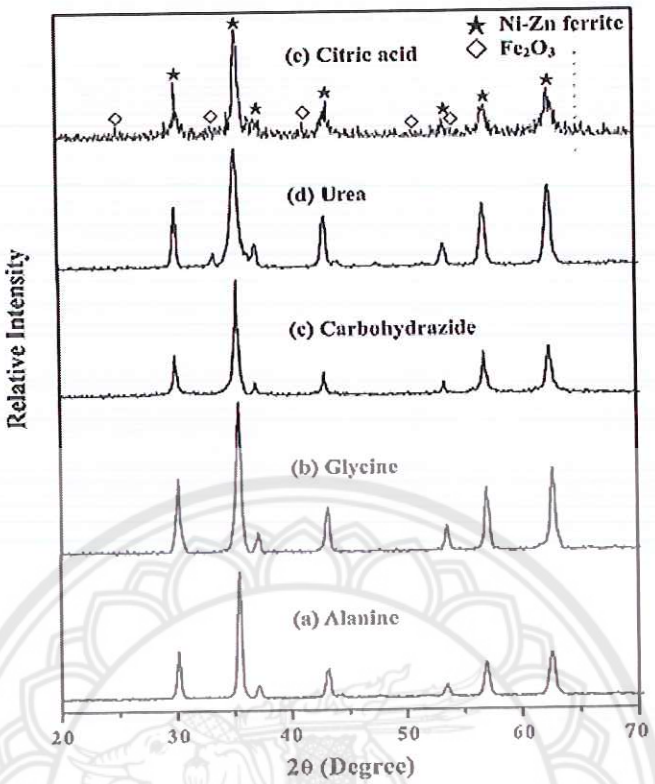

Figure 9 XRD patterns of the Ni-Zn ferrites with various organic fuels: (a) alanine (b) glycine (c) carbohydrazide (d) urea and (e) citric acid [67]

Wu, et al. [71] studied the effect of using various fuels on the structure and magnetic properties of SiO_2-doped Ni-Zn ferrite composite prepared by sol-gel combustion method. The result shows that the fuel type dramatically influenced the phase formation and electromagnetic properties of final products. The particle size for preparing its powders decreased in order: glycine route > hydrazine route > citric acid route, which are 34, 22 and 18 nm, respectively. Thus, citric acid was an effective chelating agent in producing fine ferrite powder. However, the glycine route was an effective fuel to possess the best magnetic properties with high saturation magnetization and low value of coercively.

Table 3 Effect of various fuels of the Ni-Zn ferrites prepared by the combustion technique [67]

Fuel	[a]T_m (°C)	Amount of gas produced (mole)	Crystallite size[b] (nm)	Surface area (m^2/g)	Carbon content (wt.%)	Ni^{2+} :Zn^{2+} : Fe^{3+}	M_s[C] (Am^2/kg)
Alanine	1245	20.7	38.6	24.7	1.64	0.500:0.467: 1.920	60.8
Glycine	1150	26.2	32.7	31/2	1.53	0.500:0.471: 1.922	62.4
Carbohydrazide	1380	24.0	43.7	20.6	1.87	0.500:0.462: 1.917	58.5
Urea	785	30.7	20.2	48.5	3.82	0.500:0.483: 1.936	57.2
Citric acid	725	26.2	22.7	44.1	5.75	0.500:0.490: 1.947	55.8

Note: [a]T_m the maximum combustion temperature, measured by Pt-Pt-Rh thermocouple.

[b]Crystalline size of the as-synthesized Ni-Zn ferrite powders calculated from the line broadening of the (311) XRD peak by Sherrer formula.

[c]M_s the saturation magnetization of the sintered Ni-Zn ferrite samples (950 °C/2h).

Lead free piezoelectric ceramics

Many of the piezoelectric materials used today are lead-based. The PZT family mentioned initially is the most common one. This is the binary solid solution of $PbZrO_3$ an antiferroelectric (orthorhombic structure) and $PbTiO_3$ a ferroelectric structure (tetragonal perovskite structure). PZT has the perovskite structure with the Ti^{+4} and Zr^{+4} ions at B site at random. The phase diagram shows that at high temperature PZT has the cubic perovskite structure which is paraelectric and on cooling below the curie point the structure under goes a phase change from the ferroelectric tetragonal phase to rhombohedral phase. PZT dominates the field of

piezoelectrics because of its strong piezoelectric effect, especially at the compositions near the morphotropic phase boundary $Pb(Zr_{0.52}Ti_{0.48})O_3$, where two ferroelectric phases tetragonal and rhombohedral coexist at the room temperature. The morphotropic phase boundary of PZT is almost vertical in the phase diagram, as shown in Figure 10 which maintains the excellent piezoelectric properties across a wide temperature range [48].

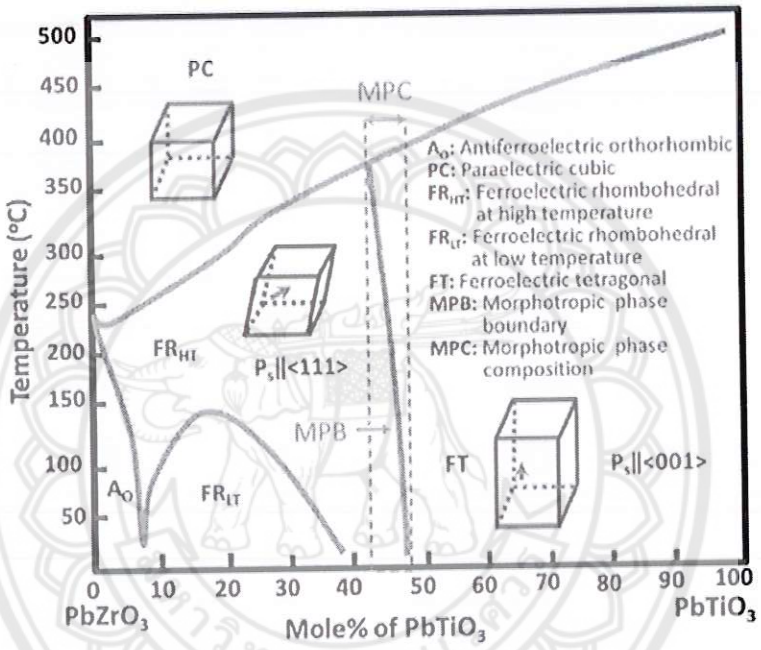

Figure 10 The phase diagram of PZT [48]

Some newer generations of lead-based piezoelectrics that exhibit exceptional piezoelectric properties have also been created by combining $PbTiO_3$(PT) with some lead-based ferroelectrics such as $Pb(Zn_{1/3}Nb_{2/3})O_3$ (PZN) and $Pb(Mg_{1/3}Nb_{2/3})O_3$ (PMN) to form solid solutions. Also, these materials show very high dielectric constants at room temperature owing to the broadening of the permittivity peak around the Curie temperature. PZT ceramics with MPB composition can also be doped with different ions and form "hard and soft" PZT is depending upon the requirements for certain applications [48].

The essential deficiency of Pb-based (PT, PZT and PMN) concerns its lead content. The amount of Pb in the usual Pb-based ceramics is more than 50 wt%, and once the Pb comes into the human body, it collects in various organs, leading potentially to serious effects to foetus, infertility, cancer and so forth. Note that not only the Pb in Pb-based compounds such as PT, PZT and PMN but also the PbO using as a raw material are known to dissolve when it is exposed to an aqueous environment However, high volatilization of PbO and its toxicity can pollute the environment and damage to human health, and then engender a terrible problem of environment pollution. However, these ceramics are toxic in the environment and damage to human health. The best way of prevention is to avoid the contact with leaded materials. Therefore, it is necessary in the search for lead-free piezoelectric materials to replace PZT ceramics.

Therefore, enormous efforts have been considerate in last decade for the development of competitive lead free counterparts, for example (K, Na)NbO_3 (KNN) based perovskite.

Potassium sodium niobate

Potassium sodium niobate (KNN) is considered as promising lead-free materials alternative to PZT a good candidate to replace PZT family. This system has an advantage of high Curie temperature (T_c~420 °C) suitable for wide temperature range of piezoelectric application. However, pure KNN solid solution exhibits relatively a low piezoelectric coefficient (d_{33}~80 pC/N) and poor remnant polarization (P_r~11 μC/cm^2). Moreover, pure KNN ceramics are very difficult to obtain at high density by traditional sintering processes because of the volatility of K^+ and Na^+ and the low phase stability at high sintering temperatures [72]. In order to improve the densification and the electrical properties of KNN ceramics, binary and ternary systems have been investigated by adding other elements.

Zuo, et al. synthesized the highly dense (1-x)($Na_{0.5}K_{0.5}$)NbO_3-x($Bi_{0.5}Na_{0.5}$)TiO_3 abbreviated KNN-BNT (x=0.005, 0.01, 0.02, 0.03, 0.05, 0.09, 0.15, 0.2, 0.8 and 1.0) solid solution ceramics. The KNN-BNT have been prepared consisted of the calcined powder and sintered ceramic at 900 °C for 5 h and 1090 °C for 2 h, respectively. The

SEM morphology of KNN-BNT ceramics was shown in Figure 11. The grain size changes from 3 to 4 μm for 0.99KNN-0.01BNT to ~0.6 μm for 0.95KNN-0.05BNT.

Figure 11 SEM micrographs of (1−x)KNN-xBNT ceramics sintered at 1090 °C with x equal to (a) 0.01, (b) 0.03 and (c) 0.05 [73]

The x-ray diffraction patterns of KNN-BNT ceramics were shown in Figure 12. All composition show pure perovskite structure. KNN was changed by adding a small amount of BNT. (1−x)KNN-xBNT ceramics at room temperature had orthorhombic structures similar to pure KNN, when $x \leq 0.02$. It becomes tetragonal when more BNT was added. However, the tetragonal symmetry remains in a limited composition range within which the tetragonality decreases with increasing the BNT content. The cubic structure starts to appear when x is greater than 0.09 until x=0.20 approximately when x continues to increase, NKN-BNT solid solutions exhibit rhombohedral structures until pure BNT composition which was known to be rhombohedral symmetry at room temperature.

(1−x)KNN-xBNT ceramics were investigated with their phase transition behavior and electrical characterization. A continuous phase transition was identified by adding a certain amount of BNT into KNN compositions, bringing about a MPB existing at 2–3 mol % BNT. Enhanced piezoelectric and electromechanical properties d_{33} =195 pC/N and k_p=43% (Figure 13) were obtained in the composition near the MPB. These compositions also have a comparable Curie temperature of 375 °C to that of PZT ceramics. These properties indicated that this system may be an attractive lead-free material for piezoelectric applications.

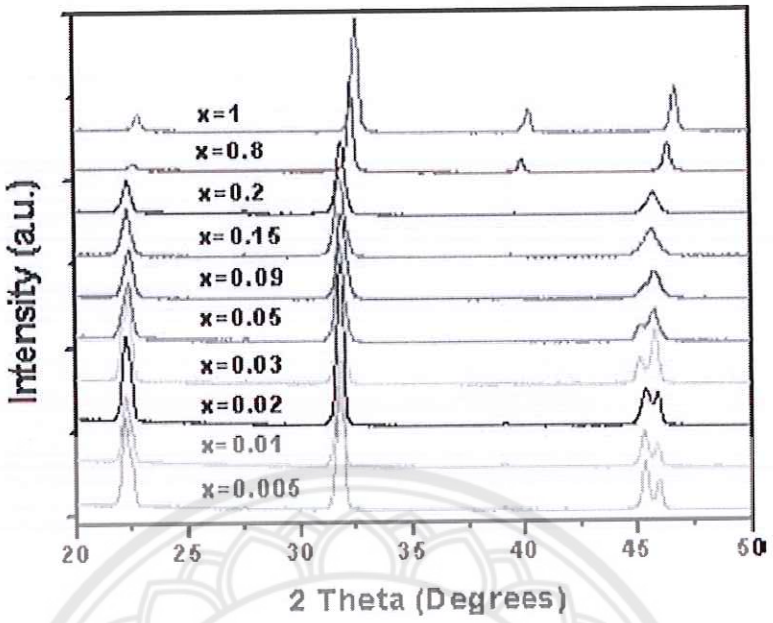

Figure 12 XRD patterns of (1-x)KNN-xBNT ceramics with x, as indicated [73]

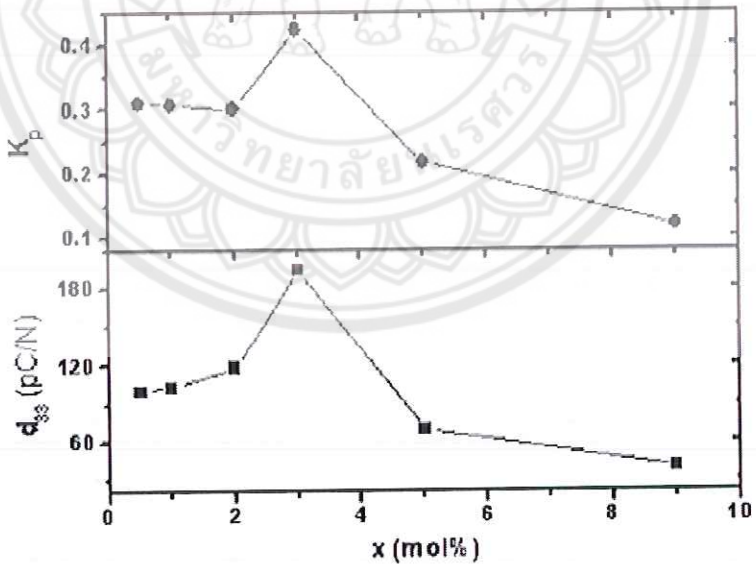

Figure 13 Piezoelectric constants and electromechanical coupling factors of (1-x)KNN-xBNT ceramics as function of the BNT content x [73]

Saito, et al. [74] presumed MPB compositions in the binary KNN- LiTaO3 (LT) system or ternary KNN-LT-LiSbO3 (LS) as shown in Figure 14. They found that the texture ceramic of the $(K_{0.44}Na_{0.52}Li_{0.04})(Nb_{0.84}Ta_{0.10}Sb_{0.06})O_3$ (L4FT) synthesized by the reactive template grain growth (RTGG) technique attains excellent piezoelectric constant d_{33} of ~400 pC/N.

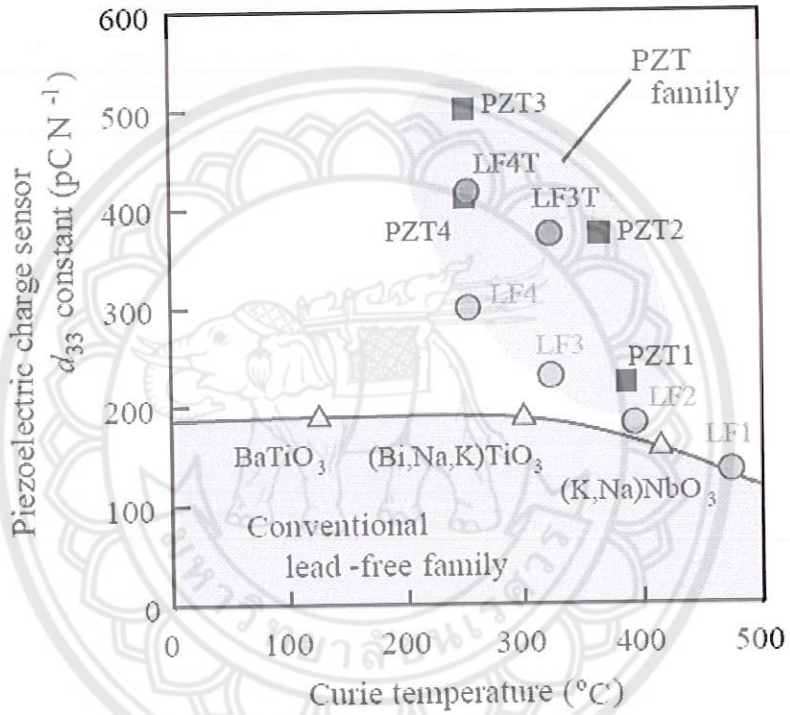

Figure 14 Piezoelectric sensor performances for the lead-free piezoelectric ceramics [74]

Jiang, et al. [75] reported the piezoelectric properties of (1-x) $(K_{0.44}Na_{0.52}Li_{0.04})(Nb_{0.84}Ta_{0.10}Sb_{0.06})O_3$-x$BiFeO_3$ (x=0, 0.002, 0.004, 0.006, 0.008 and 0.01) fabricated by conventional mixed-oxide technique using a calcination temperature of 880 °C for 6 h and a sintered temperature of 1135 °C for 3 h. The x-ray diffraction patterns of KNN-BNT ceramics were shown in Figure 15. All samples exhibited pure perovskite structure and no secondary phase could be found in all samples. The (1-x)(KNLNTS)-xBF ($x \leq 0.004$) ceramics are single perovskite phase

with single orthorhombic crystal system. However, the symmetry changes rapidly with the addition of BF. The XRD patterns near at x = 0.004–0.006 show mixed phases. When x ≥ 0.008, it becomes a tetragonal perovskite structure. This result indicates that the transitional point for the structure change can be certified to be near x = 0.004–0.006. So a morphotropic phase boundary (MPB) between the orthorhombic and tetragonal ferroelectric phases of the (1-x)(KNLNTS)-xBF ceramics was identified in the composition range of 0.004–0.006.

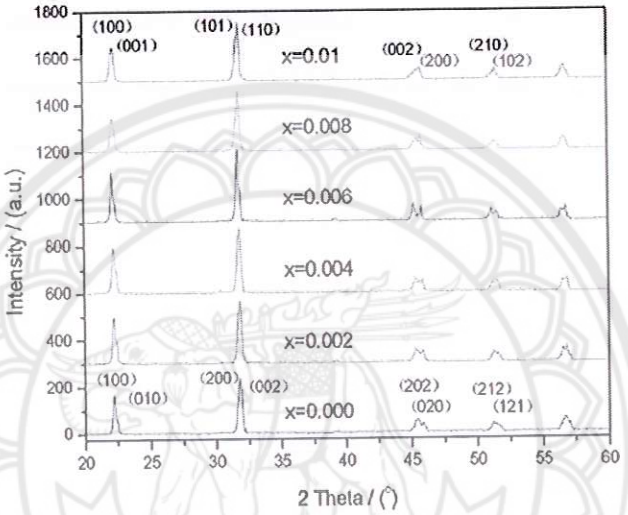

Figure 15 XRD patterns of BF doped KNN–LS–LT ceramics sintered [75]

Table 4 Density and electrical properties of KNLNTS–BF ceramics [75]

x	0	0.002	0.004	0.006	0.008	0.1
Bulk density (g/cm^3)	4.62	4.71	4.79	4.80	4.79	4.78
d_{33} (pC/N)	92	205	206	246	118	88
k_p	0.23	0.38	0.42	0.43	0.24	0.21
Q_m	94	138	130	94	130	140
Tan δ (%) (at 1 kHz)	4.62	2.88	2.86	1.96	3.05	3.24
ε_r (at 1 kHZ)	1096	1410	1494	1871	1611	1702
T_{o-t} (°C)	115	85	70	35	<25	<25
T_c (°C)	320	305	285	285	265	235

The piezoelectric properties of (1-x)(KNLNTS)-xBF ceramics were shown in Table 4. The best piezoelectric and electromechanical properties of d33 = 246 pC/N and kp = 43% appear at x = 0.006.

Hagh, et al. [76] synthesized $(K_{0.44}Na_{0.52}Li_{0.04})(Nb_{0.84}Ta_{0.10}Sb_{0.06})O_3$ system by two possible routes, namely perovskite and mixed oxides route and studied the effect of humidity and oxygen flow rate during sintering. In case of perovskite route using a sintering temperature of 1150 °C for 1 h. It was found that piezoelectric coefficient, remnant polarization and coercive field were 300 pC/N, 18 $\mu C/cm^2$ and 8.4 kV/cm, respectively. The samples were prepared under the following special conditions; (i) the raw materials were heat treated at 220 °C for 24 h, (ii) the powder process performed in glove box with Ar gas flowing and (iii) the samples were sintered in high O_2 atmosphere (360 cm^3/min). However, under ordinary conditions, KLNLTS ceramics exhibited a low electric properties as shown in Table 5.

Table 5 Processing property relationships for KNLNTS ceramics [76]

Property/processing step	Lab atmosphere perovskite rt.	High flow rate O_2 controlled atmosphere perovskite rt.	High flow rate O_2 mixed oxide w/high purity precursors
Relative permittivity, ε_{33}^T @ 1 kHz and RT	745	1590	~1650
Dielectric loss, tan δ - 1kHz @ RT (%)	3.5	1.7	~2
Piezoelectric charge coefficient, d_{33} (pC/N)	145	300	340-370
Planar coupling coefficient, k_p (%)	28	44	48
Remnant polarization, P_r ($\mu C/cm^2$) @ RT	14	22	28-30
Relative density (%)	92	96	>97
Coervice field, E_c (kV/cm)	13.3	8	8.8

The temperature dependence of the dielectric constant (ε_r) of KNLNTS ceramics measured at the frequency of 1 kHz. The temperature dependence of the dielectric constant of KNLNTS ceramics exhibited two peaks which corresponded to the orthorhombic-tetragonal phase transition (T_{o-t}) at 31 °C, and the tetragonal-cubic phase transition (T_c) at 264 °C (Figure 16). The dielectric constants (ε_r) at T_{o-t} and T_c were ~1175 and ~8000 , respectively.

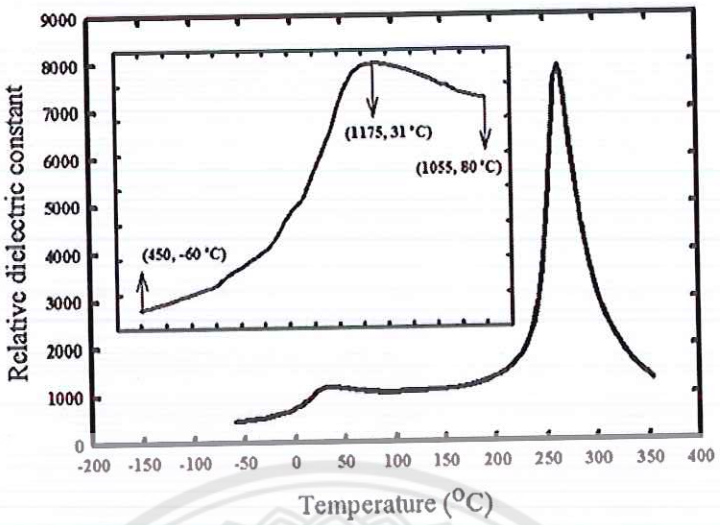

Figure 16 Variation of low-field 1kHz relative dielectric constant with temperature in $(K_{0.44}Na_{0.52}Li_{0.04})(Nb_{0.84}Ta_{0.1}Sb_{0.06})O_3$ [76]

CHAPTER III

MATERIALS AND METHOD

In this chapter explains the fabrication and characterization of KNLNTS ceramics with Fe_2O_3 doping. All powders fabrications were prepared by the solid state combustion method. The characterizations of these powders were observed using XRD and SEM. The ceramics were characterized to find out their properties such as physical properties, phase formation, microstructure, electrical and magnetic properties. The details are presented in the following sections.

Powders and Ceramics Preparation

KNLNTS ceramics with Fe_2O_3 doping (0-1.0 wt.%) were fabricated by the solid state combustion method with glycine as the fuel. Reagent grade oxide, carbonate or nitrate powders of $KHCO_3$ (%99.5), $NaNO_3$ (%99.5), Li_2CO_3 (%99.5), Nb_2O_5 (%99.5), Ta_2O_5 (%99.5) and Sb_2O_3 (%99.5) were used as raw materials. The raw materials were mixed in stoichiometric ratio and ball milled in ethanol for 24 h. The suspensions were dried and then sieved to obtain fine powders. The powders were then mixed with glycine ($C_2H_5NO_2$) in a ratio of 1:0.56 in an agate mortar and the mixed powders were calcined at 650°C for 2 h. The calcined powders were mixed with Fe_2O_3 (%99.5) at various compositions (0-1.0 wt.%) and 3 wt% of polyvinyl alcohol (PVA) solution. Then, they were ball milled again for 24 h. After that, the mixed solution was dried, then crushed and sieved. These powders were pressed into disks of 15 mm in diameter and 10 mm thick under a pressure of 80 MPa. Subsequently, the disks were sintered at 1130°C for 2 h.

Sample Characterization

The following section addresses the main characterization techniques used to investigate the phase formation, morphology, particle size, microstructure, physical properties and dielectric property of the samples in this study. They are described below.

X-ray diffraction (XRD) Technique

The X-ray diffraction (XRD) was used to identify the optimum firing temperatures, for phase identification, quantitative analysis of the mixtures of phases, and also to determine the crystal structure of the samples at room temperature, in both powder and ceramic forms. The X-ray diffractometer (Philips model X'Pert Pro) with Cu Kα radiation at 20 kV was employed as shown in Figure 17. Each sample was scanned for a 2θ range from 10°-60°. Lattice parameters of sample were determined from X-ray powder diffraction database from ICDD. The crystallite size of the calcined powder and ceramics grain size were also determined using the XRD line broadening as derived by Scherer equation [77];

$$B_{crystallites} = \frac{k\lambda}{L\cos\theta} \tag{5}$$

Where B is a broadening of the diffraction line measured at half its maximum intensity, L is the average crystallite size and k is a constant

The relative amounts of the perovskite and pyrochlore phases were calculated from the intensities of major X-ray reflections of the pyrochlore phase as perovskite phase using the equation proposed by Swart and Shrout [78];

$$\%Perovskite = \frac{I_{perovskite}}{I_{perovskite} + I_{pyrochlor}} \times 100 \tag{6}$$

Where $I_{perovskite}$ refers to the intensity of the peak of the perovskite phase and $I_{pyrochlore}$ refers to the intensity of the highest peak of pyrochlore phase.

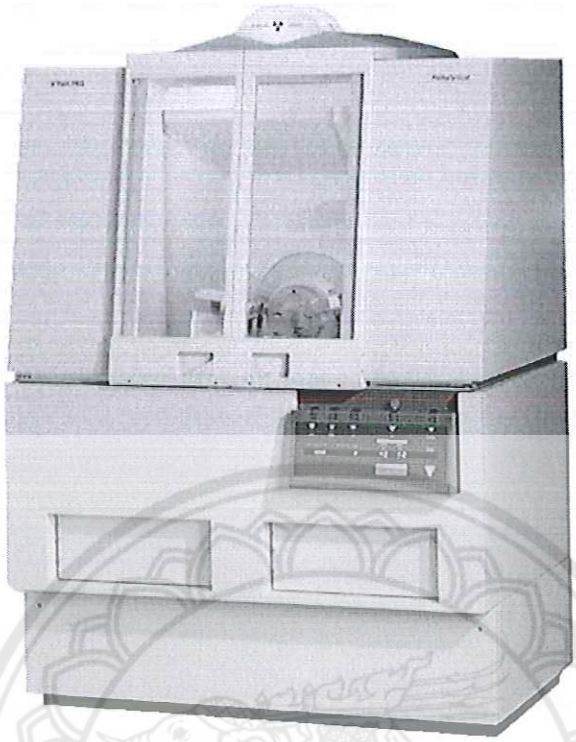

Figure 17 X-ray diffractometer [79]

Scanning electron microscopy (SEM)

Microstructural characterization of sample surface using scanning electron microscopy (SEM) (Figure 18) was performed to determine the grain size and the presence of porosity. Average grain size of the sintered ceramics were estimated by using a linear intercepting method, where random linear lines (L) were drawn on each SEM micrograph and the number of the intercepts which the grain boundary makes with the line (N). The average grain size (D) was determined from measurements along random lines using the equation [80];

$$D = \frac{L}{N} \tag{7}$$

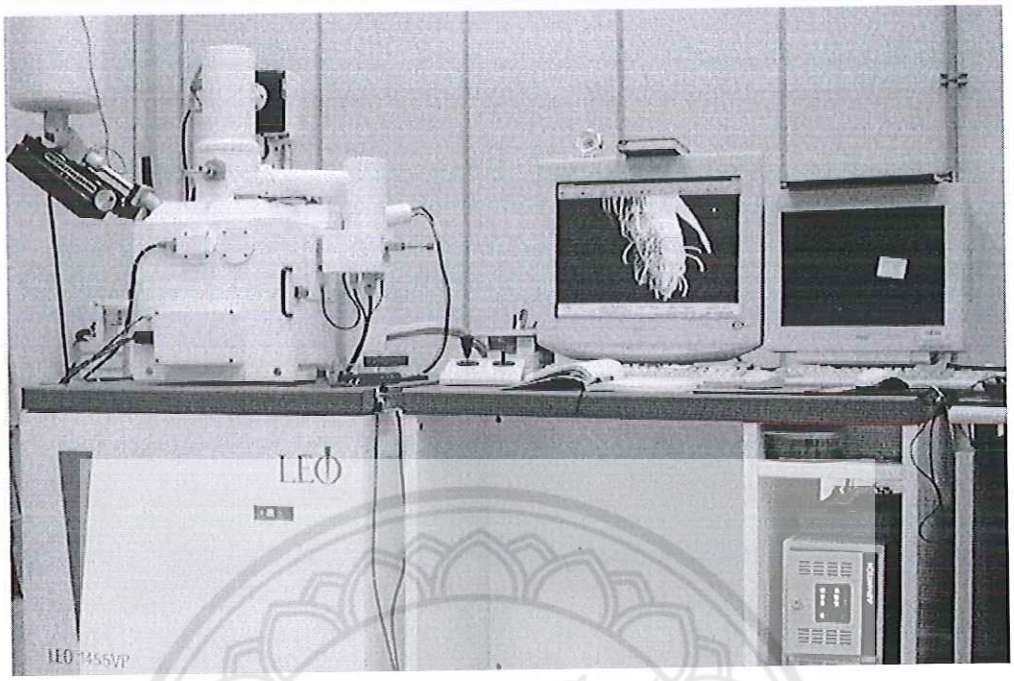

Figure 18 Scanning electron microscopy [79]

Transmission electron microscopy (TEM)

Transmission electron microscopy (TEM) (Figure 19) was employed to investigate the morphology of the powders. Samples for TEM were prepared by grinding, dispersing them in isopropyl alcohol and then depositing the sample by pipette onto 3 mm holey copper grids for observation by TEM (FEI, Technai G2).

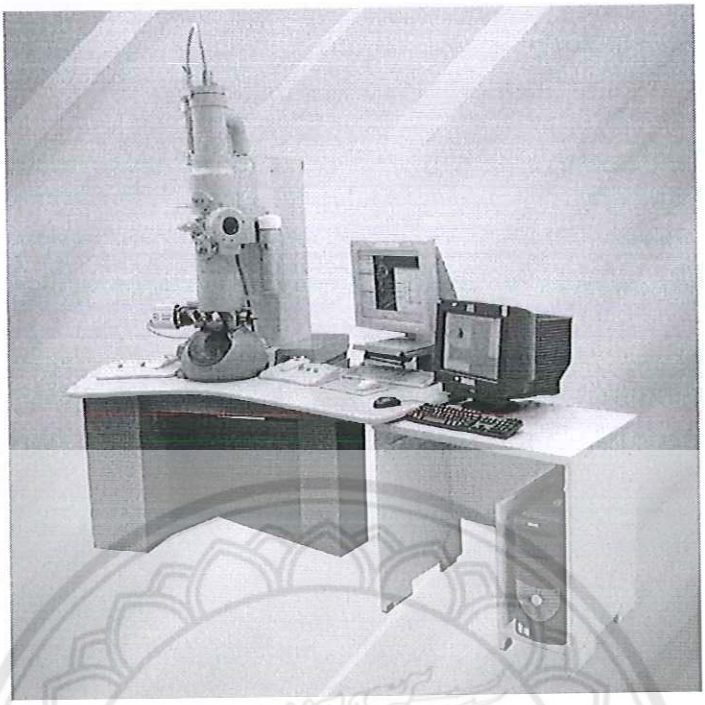

Figure 19 Transmission electron microscopy [79]

Densification analysis

The method of measuring the density of a piece of ceramics material usually described in standards is based on the Archimedes principle. This principle stated the weight of an object in a fluid equals it's by weight minus the buoyant force (or the weight of the fluid displaced). However, it is usual to measure open porosity levels at the same time by ensuring that during immersion liquid can penetrate all parts of the specimen through the open porosity. Typical procedures are;

1. Dry specimen(s) in air at 110 ºC, store in a desiccator, weigh when cold (mass W_1)

2. Boil in distilled water for a period, typically 3 hours and leave it for 1 night

3. Weigh immersed in water (W_2) and then weight during immersion liquid can penetrate all parts of the specimen through the open porosity (W_3).

4. Calculate follow this equation:

$$\rho_c = \frac{W_1 \rho_w}{W_3 - W_2} \tag{8}$$

where, ρ_w is the density of water at room temperature (g/cm^3) and is the density of sample at room temperature (g/cm^3); however the density of water is slightly temperature dependent

$$\rho_w = 1.0017 - 0.0002315T \quad (9)$$

Moreover, the fired shrinkage of all sintered ceramics were measured from the percentage diameter change with respect to the original diameter (l_0) before sintering;

$$Shrinkage(\%) = (\frac{l_1 - l_0}{l_0})x100 \quad (10)$$

where l_1 is diameter of pellet before sintering (mm),
l_0 is diameter of pellet after sintering (mm)

Dielectric measurement

The dielectric properties of the sintered ceramics were studied as functions of both temperature and frequency with an automated dielectric measurement system. The measurement system which measured the dielectric properties consisted of a LCR meter (Agilent 4263B). The dielectric properties were determined over a temperature range from room temperature to 200 °C with different frequencies (3 frequency of 1 kHz, 10 kHz and 100 kHz). The dielectric constant (ε_r) was calculated with the following equation,

$$\varepsilon_r = \frac{Cd}{\varepsilon_0 A} \quad (11)$$

where ε_0 is the permittivity of free space,
C is the capacitance,
D is the thickness of the sample,
A is the area of the sample.

P-E measurement

P-E measurement was made using high voltage amplifier (Trek), precision High Voltage Interface (HVI, Radiant Technologies), precision LC (Radiant Technologies) and computerized control and data acquisition. The sample is placed in a High Voltage Test Fixture chamber (HVTF) chamber in bottom half of the fixture. A copper electrode fixed in the bottom of the chamber contacts the electrode on the bottom of the sample. The bottom chamber is sealed so it may be filled with insulating oil to protect the sample from the arcing that may occur in open air. The system is an automated device intended for measuring the polarization of materials induced by a single triangle wave. It can prevent the excess voltage and current during a sample breakdown from exceeding the current canceling capability of the virtual ground circuitry on the tester input. During the measurement, an electric field of 30 kV/cm based on the coercive field was applied to a sample which immersed in a silicone oil to prevent the breakdown of the sample.

Piezoelectric properties measurement

The optimum poling conditions were determined by poling the KNLNTS ceramics with applying DC field of 3 kV/mm in a stirred oil bath at 80°C for a time period 30 minutes. The piezoelectric constant (d_{33}) was measured using a quasi-static piezoelectric d_{33} meter. The piezoelectric constant (d_{33}) measurements were made directly after poling and after 24 hours. Measurements were conducted at a drive frequency of 100 Hz.

CHAPTER IV

FABRICATION OF KNLNTS CERAMICS WITH Fe_2O_3 Doping CERAMICS BY THE SOLID STATE COMBUSTION TECHNIQUE

The phase formation of Fe_2O_3-doped KNLNTS (KNLNTS-xFe) ceramics sintered at 1130°C for 2 h with various x content ($0 \leq x \leq 1.0$ wt%) was examined by the X-ray diffraction technique as shown in Fig.1 (a). The XRD pattern in 2θ range of 10-60° displayed a single perovskite symmetry when using Fe_2O_3 doping between 0 and 0.6 wt% (Fig 20 (a) I-IV) which matched with the JCPDS files number 71-0945 [29], 71-2127 [30] and 08-0212 [31]. This result implied that Fe_2O_3 enters into the lattice structure of the KNLNTS ceramics during sintering. While, secondary phases of $FeNbO_4$ and $FeTaO_4$ were detected in the samples doped with Fe_2O_3 higher than 0.6 wt% (Fig 20 (a) V, VI). The percentage of the perovskite phase in these ceramics is listed in Table 6. Further XRD consideration at 44-47° using a very low scanning rate (step size 0.005796°, time/θ 3.565 s, scan speed 0.050398°/s) for all compositions is displayed in Fig. 20 (b). Generally, it is acknowledged that in the 2θ range of 44-47° the character of a tetragonal phase (T) is identified by dual splitting peaks of (002) at lower angle and (200) at higher angle because $c > a = b$ [29] while an orthorhombic phase (O) is characterized by two split peaks of (202) at lower angle and (020) at higher angle because $a \approx c > b$ [30]. In the case of characteristic of cubic phase (C), it is identified by a single peak of (200), at 2θ in the range of 44-47° [31]. For ideal intensity ratio of the dual peaks, it shows the volume ratios $I_{(202)}/I_{(020)}$ orthorhombic

phase and $I_{(002)}/I_{(200)}$ tetragonal phase of about 2 and 1/2, respectively. While, the value is around 1 for mixture between orthorhombic and tetragonal phases with equivalent content [32]. In this study, the phase formation of KNLNTS ceramic with undoped Fe_2O_3 exhibited the dual peaks at around 45° and the ratio was 1.13 (Table 6). This indicated that the structure is an orthogonal phase (the combination of the orthorhombic and tetragonal structures) (Fig. 20 (b) I), which was similar to the previous reported work [15]. The dual peaks shifted evidently to a lower angle and the intensity of first peak (I_{FP}) peak increased, while, the intensity of second peak (I_{SP}) gradually reduced when x doping increased from 0 to 0.6 wt%. The ratio of I_{FP}/I_{SP} increased from 1.13 to 1.76 when Fe_2O_3 doping increased from 0 to 0.6 wt% (Table 6) which indicated a higher orthorhombic phase dominated in these samples (Fig. 20 (b) I-IV). At Fe_2O_3 doping of $0.8 \leq x \leq 1.0$ wt%, the dual peaks started to fuse into a single (200) peak. This peak shifted slightly to a higher angle and the intensity of this peak was rather steady. These results indicated that a cubic phase began to occupy these samples and the quantity of cubic phase increased with increased amounts of x (Fig. 20 (b) V, VI) [31].

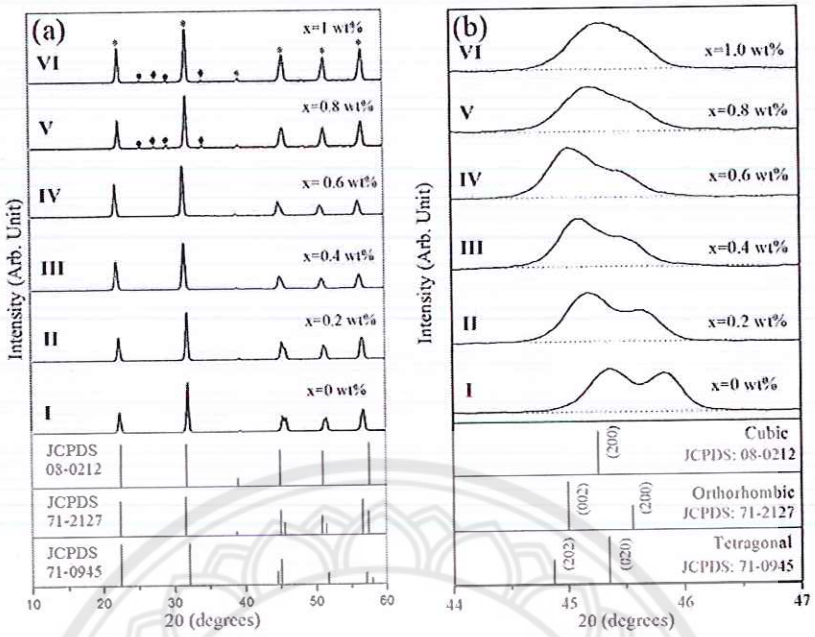

Fig. 20. XRD patterns of the KNLNTS ceramics as a function of Fe_2O_3 doping in 2θ range of (a) 10-60° and (b) 44-47 ° (*) perovskite (•) $FeTaO_4$ and (♦) $FeNbO_4$.

Fig. 21 (a)-(f) show the surface microstructure of KNLNTS ceramics with various Fe_2O_3 doping (0-1.0 wt%). The SEM image observation found that all samples presented a rectangular shaped grain and an evident grain boundary. As seen in Fig. 21 (a), the undoped KNLNTS ceramic displayed large porosity on surface of this ceramic. The porosity was reduced when Fe_2O_3 doping increased from 0.2 to 0.6 wt% (Fig. 21 (b) - (d)), but increased with higher Fe_2O_3 doping (Fig. 21 (e) and (f)). The grains of all samples exhibited an uneven size and the grain size was distributed widely throughout the surface. The average grain size increased from 1.52 to 2.10 μm, depending on the Fe_2O_3 content from 0 to 0.6 wt%, and then reduced for higher Fe_2O_3 content. The density of the KNLNTS ceramics increased from 4.42 to 4.65 g/cm^3 (93.5-96.1% of theoretical value) with increasing Fe_2O_3 content until 0.6 wt.%.

The average grain sizes as well as the density of KNLNTS ceramics are summarized in Table 6.

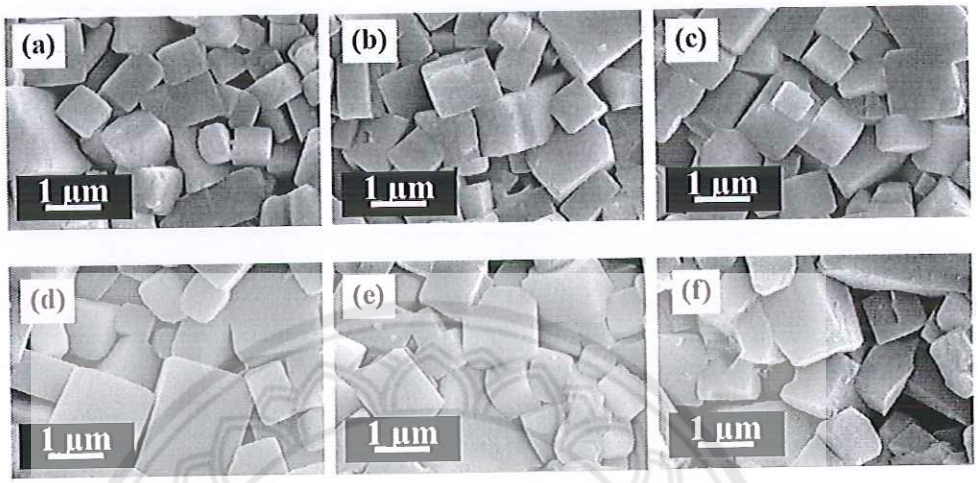

Fig. 21. SEM image of surfaces of KNLNTS ceramics as function of Fe_2O_3 doping: (a) x = 0, (b) x = 0.2, (c) x = 0.4, (d) x = 0.6 (d) x = 0.8 and (f) x = 1.0 wt%.

Table 6 % Peroveskite, I_{FP}/I_{SP}, grain size and density of KNLNTS ceramics with a function of Fe_2O_3 concentration.

Fe_2O_3 doped (wt.%)	% Peroveskite	I_{FP}/I_{SP}	Grain size (µm)	Density (g/cm^3)	Relative density (%)
0	100	1.13	1.52±0.25	4.42	93.5
0.2	100	1.52	1.61±0.28	4.57	94.3
0.4	100	1.55	1.78±0.25	4.63	95.7
0.6	100	1.76	2.10±0.22	4.65	96.1
0.8	98	-	1.88±0.21	4.62	95.3
1.0	97	-	1.75±0.26	4.59	94.8

The grain growth formation and the densification deportment associated with Fe_2O_3 doping can be explained in terms of defect chemistry and the creation of oxygen vacancies. Both theoretically and experimentally, it is well known that the better atomic diffusion occurs during sintering process because of the number of vacancies formed. Moreover, the dopant is cationic that creates and increase vacancies which benefit in the development of morphology and densification. For the system under investigation, the defect equation is written as the following:

$$Fe_2O_3 = 2Fe_M^{\cdot} + 3O_O^x + 2V_O^{\cdot\cdot}$$

It can be noted that the above defect equation only assumed ionic defect reciprocation. Furthermore, it was assumed that Fe ions preferentially substituted in B sites (Nb, Ta and Sb). The latter assumption was based on the fact that the ionic radius of Fe^{3+} (0.645Å) was closer to the ionic radius of Nb^{5+} ion (0.64 Å), Ta^{5+} ion (0.64 Å) and Sb^{5+} ion (0.6 Å). In addition, the ratio of cationic radius to anionic radius (O^{2-}=1.40 Å) would exclude the Fe ion from residing at A site due to the instability of the structure [33]. Based on the nominal charge of Fe^{3+}, the amount of oxygen vacancies could be approximated from this equation and increased with increasing amount of Fe^{3+} ions substituting B sites (M; Nb, Ta and Sb). Therefore, the proper amount of Fe_2O_3 doping leads to generation of oxygen vacancies, which help to enhance the mass transfer in the sintering process and strongly promote grain growth and densification. However, higher Fe_2O_3 doping led to reduce of grain size and density. B.Yang et al [34] reported that, when Fe_2O_3 is doped above the solubility limit, there is a segregation of excessive quantities of Fe ions at the boundaries, which can produce a secondary impure phase and displays a close-packing role between

grains. The results of density were corresponded to the results of morphology and phase formation investigation.

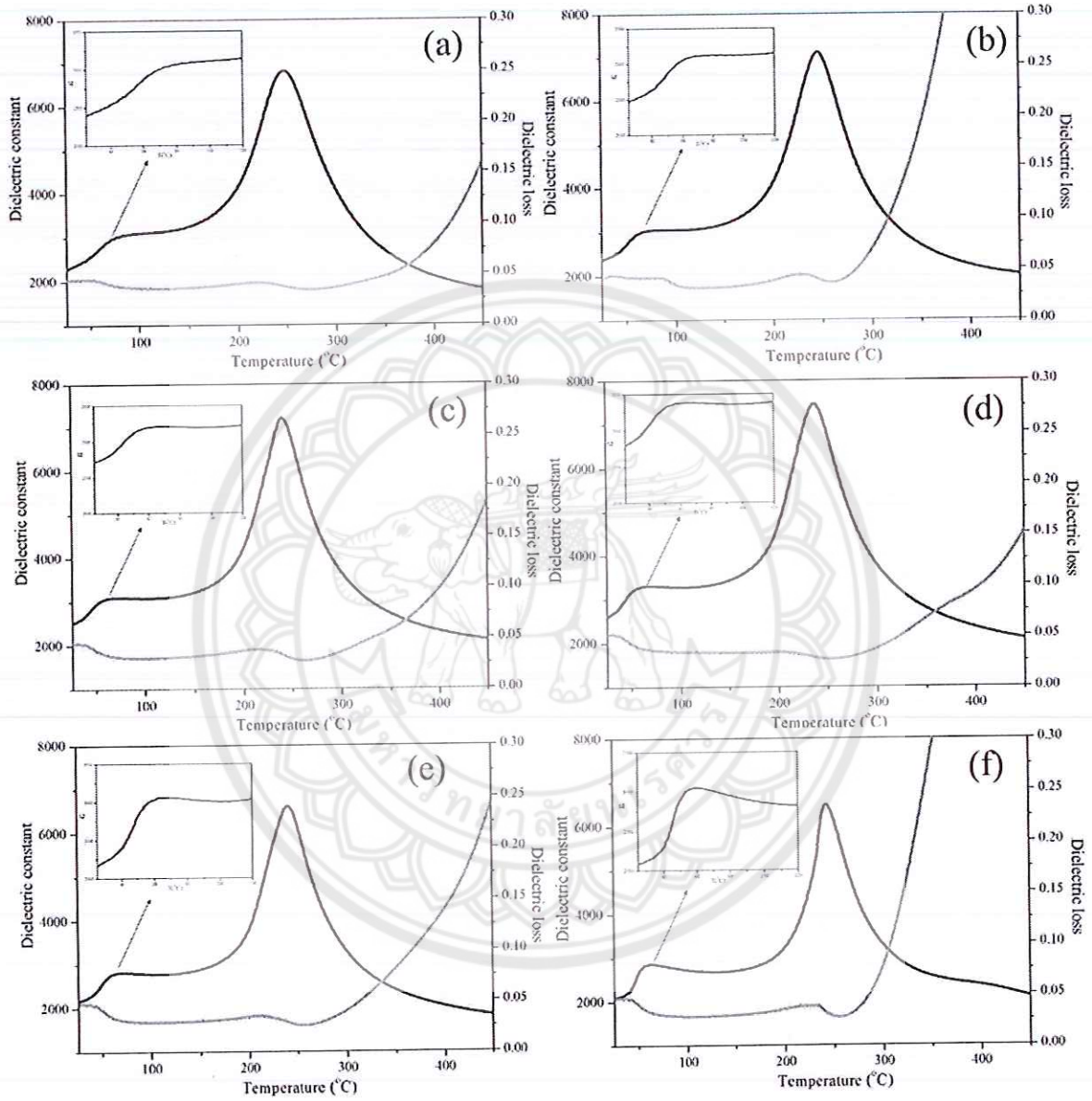

Fig. 22. The temperature dependence of dielectric properties of KNLNTS ceramics at Fe_2O_3 content of (a) 0 wt%, (b) 0.2 wt%, (c) 0.4 wt%,(d) 0.6 wt%,(e) 0.8 wt% and (f) 1.0 wt%.

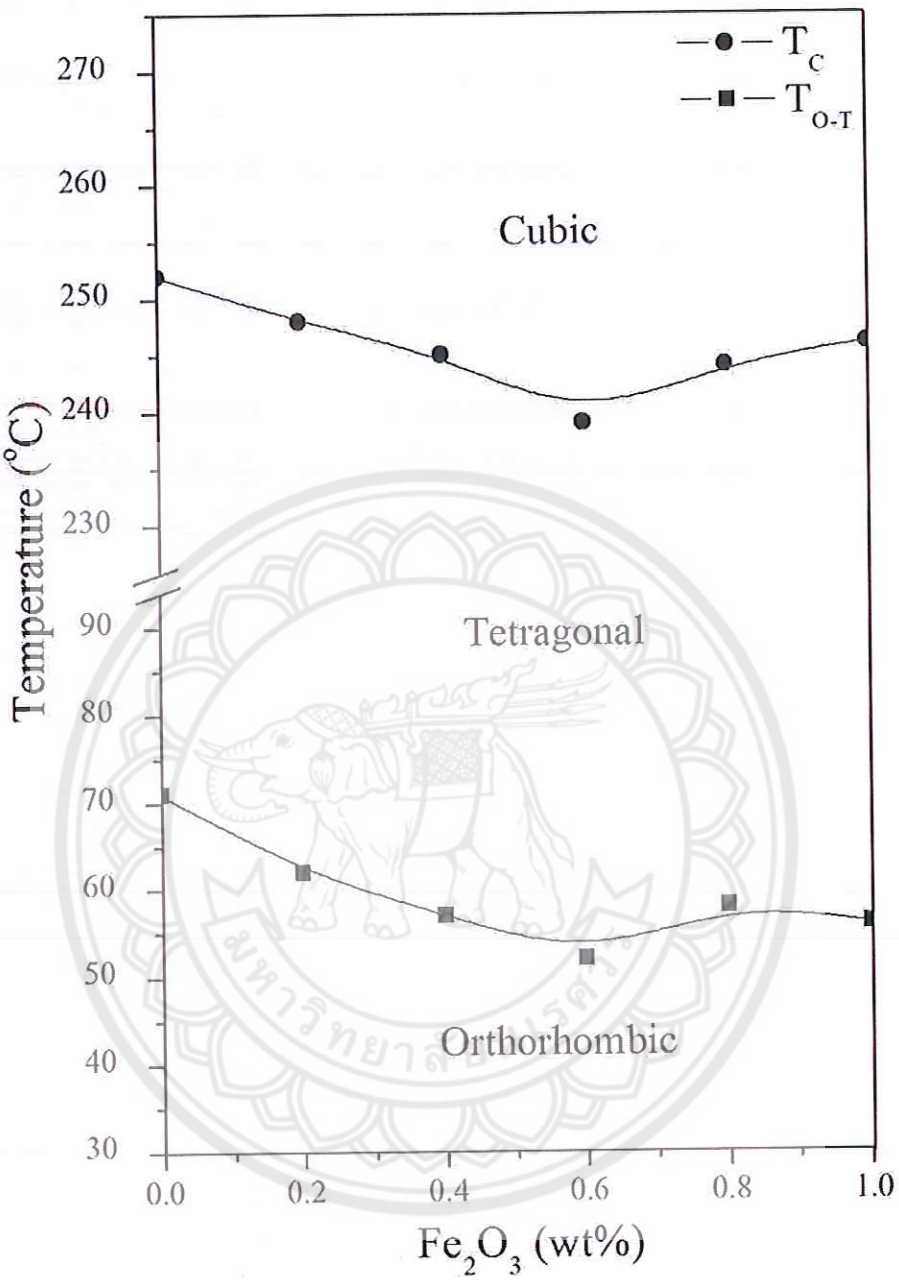

Fig. 23. Phase diagram of KNLNTS ceramics with adding different Fe_2O_3 content.

Fig. 22 shows the temperature dependence of the dielectric behavior of KNLNTS ceramics with Fe_2O_3 doping from 0 to 1.0 wt% measured at frequency of 1 kHz with a sample heating speed of 1°C/min. It is evident that all KNLNTS samples showed two dielectric anomalies. The first peak occurring at around 60°C corresponded to phase transition from orthorhombic ferroelectric phase to tetragonal ferroelectric phase (at T_{O-T}, phase transition temperature). The second peak at high temperature (around 250°C) related to the phase transform from tetragonal ferroelectric phase to cubic paraelectric phase (at T_C, Curie temperature) [5, 12, 15, 35]. The tetragonal-orthorhombic phase transition peak was stronger by increase of Fe_2O_3 content, which is shown clearly in the insets of Fig. 22 (a)-(f). This result is different from the substituted $LiSbO_3$ in to KNN ceramics which it was weaker by higher the substitution [36]. The T_{O-T} and T_C of these samples shifted to low temperature when Fe_2O_3 doping increased up to 0.6 wt% and then shifted to high temperature, as represented in Fig 4. Many researcher groups attributed the variations of T_{O-T} and T_C of KNN-based ceramics with related phase transformations [36-40]. It can be realized that a partial substitution at A-site of KNN-based ceramics affect T_C to increase and T_{O-T} to decrease [37]. For a partial substitution at B-site, T_C and T_{O-T} of KNN-based ceramics decrease rapidly [38, 39]. In addition, the partial substitution of both A-site and B-site in KNN-based ceramics is result in different rates of linear decrease in T_C and T_{O-T} with phase evolutions of $O \rightarrow O + T \rightarrow T$ at room temperature (T_r) reported by D. Lin et. al. [36]. Afterward, X. Shang et.al [40] reported relation of phase formations and phase transition temperatures of $N_{0.5}K_{0.5}$LNSTx + Mn ceramics substitution by Ta^{5+} at B-site. It was found that the T_{O-T} showed obvious "V" type variation while T_C decreased monotonically. They described the obtaining of "V"

type variation in T_{O-T} by exhibiting the phase transformations of $O \rightarrow O + T \rightarrow O$ at T_r with increasing Ta^{5+} content. In this study, the T_{O-T} and T_C of these samples shifted to low temperature when Fe_2O_3 doping increased up to 0.6 wt% and then shifted to high temperature, as represented in Fig 4. So, the variations of both T_{O-T} and T_C of KNLNST with doping Fe_2O_3 demonstrated the "V" type evolution as seen in Fig 4. This variation may be resulted from the phase evolution of $O + T \rightarrow higher\ O + lower\ T \rightarrow psuedo\ Cubic$ at T_r, which was exhibited by XRD result. The exact explanation of this phenomenon is required in future work. The dielectric constant at T_r (ε_r) and at T_C (ε_m) were found to increase with increasing Fe_2O_3 content up to 0.6 wt% and then dropped in value when Fe_2O_3 was continually added > 0.6 wt% (Table 7). The maximum ε_r and ε_m of 2782 and 7520 were obtained from the sample doped 0.6 wt% of Fe_2O_3. The tanδ values at T_r and T_C were listed in Table 7. The dielectric properties were corresponded to phase formation, morphology and density results.

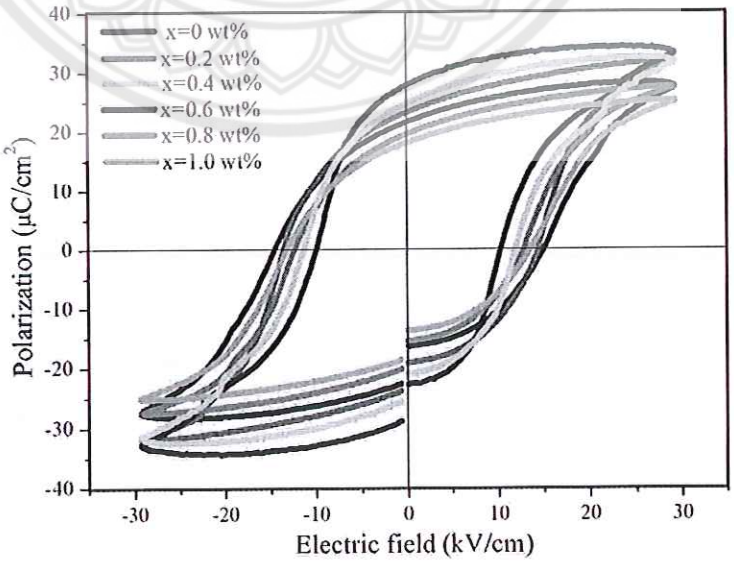

Fig. 24. Plots of electric polarization against electric field of KNLNTS ceramics with adding various Fe_2O_3 concentration.

To estimate the effect of Fe_2O_3 doping on the ferroelectric behavior, P-E hysteresis loops of these samples were measured at room temperature under the maximum applied electric field 30 kV/cm and are shown in Fig. 24. The P-E hysteresis loops of all compositions displayed well saturated and fairly slim symmetric loops that indicated typical ferroelectric behavior. The remnant polarization (P_r) and the coercive field (E_c) with doped Fe_2O_3 (0-1.0 wt%) are listed in Table 7. For the undoped KNLNTS ceramic, the values of remnant polarization (P_r) and coercive field (E_c) were about 19.9 $\mu C/cm^2$ and 14.9 kV/cm, respectively. By additive of Fe_2O_3 $\leq$0.6 wt%, it is clearly seen that the P_r values continuously increased and E_c values reduced as listed in Table 7. When, the Fe_2O_3 content was higher than 0.6 wt%, the P_r and E_c values represented the opposite trend (Table 7). The maximum P_r value (27.9 $\mu C/cm^2$) and the minimum E_c value (9.9 kV/cm) were obtained at the Fe_2O_3 concentration of 0.6 wt%. The analysis of ferroelectric characteristics can be calculated from the degree of squareness (R_{sq}) of the P-E loop. It can be made using $R_{sq} = (P_r/P_s)+(P_{1.1Ec}/P_s)$, where, P_s is the saturated polarization obtained at some finite field strength below the dielectric breakdown and $P_{1.1Ec}$ is the polarization at the field equal to $1.1E_c$. $R_{sq} = 2.00$ is an excellent square loop [35]. According to this calculation, the squareness values of the samples increased continuously from 0.95 to 0.99 when Fe_2O_3 concentration increased from 0 to 0.6 wt% and then drop in value as listed in Table 7. This indicated that ferroelectric behavior increased with increasing the doped Fe_2O_3 content up to 0.6 wt%. More Fe_2O_3 doping in KNLNTS ceramics led to a reduction in remnant polarization and squareness, indicating a reduction of ferroelectricity [41]. It has to be noted that due to the P-E loops are not colsed for any

of the compositions, the absolute values of ferroelectric properties such as P_r, E_c and R_{sq} in this work are inaccurate.

The piezoelectric constant (d_{33}) of KNLNTS ceramics with different doped Fe_2O_3 level from 0-1.0 wt% is listed in Table 7. It was found that the piezoelectric constant d_{33} increased from 195 pC/N to 311 pC/N when the Fe_2O_3 content increased from 0 to 0.6 wt %. After that, the d_{33} value reduced with further increase in the Fe_2O_3 concentration. The 0.6 wt% Fe_2O_3 doped ceramic was attained the highest piezoelectric constant d_{33} of 311 pC/N. It is well known that the d_{33} value of KNN-based ceramics can be increased by doped and substituted cation owing to the formation of polymorphic phase transition (PPT) at around T_r [36]. For the above discussion, the XRD result and the temperature dependent dielectric measurement confirmed that a PPT of KNLNTS ceramic with Fe_2O_3 doping was observed by Fe_2O_3 content at 0.6 wt% due to the coexistent O+T phases at T_r and the nearest T_r of T_{O-T} were occurred. So, this sample gave rise to increase piezoelectric coefficient. It should be noted that the piezoelectric property of undoped KNLNTS ceramics prepared by the solid state combustion technique is higher than the KNLNTS ceramics prepared by the conventional technique (92 pC/N) [12]. In the case of Fe_2O_3 doping at 0.6 wt% KNLNTS ceramics fabricated by the solid state combustion technique, the electrical properties such as piezoelectric and ferroelectric properties were higher than the pure KNLNTS ceramic synthesized by mixed-oxide route using special conditions [13] and KNL-NTS ceramic doped 0.3 mol% Fe_2O_3 prepared via conventional solid state reaction technique [17]. Hence, the solid state combustion technique and Fe_2O_3 doping should be considered as an alternative way for improving the electrical properties of KNN-based ceramics.

Table 7 Dielectric, ferroelectric and piezoelectric properties of KNLNTS ceramics with a function of Fe_2O_3 concentration.

Fe_2O_3 doped (wt.%)	ε_r	tanδ at T_r	ε_m	tanδ at T_C	P_r ($\mu C/cm^2$)	E_c kV/cm	R_{Sq}	d_{33} (pC/N)
0	2350	0.045	6786	0.036	19.9	14.9	0.95	195
0.2	2492	0.042	7120	0.040	22.4	13.5	0.96	235
0.4	2729	0.046	7256	0.032	24.6	11.3	0.98	274
0.6	2782	0.050	7520	0.026	27.9	9.9	0.99	311
0.8	2285	0.065	6625	0.027	19.9	12.2	0.93	203
1.0	2226	0.044	6471	0.029	18.1	13.1	0.91	120

The magnetic hysteresis loops (M-H loop) of KNLNTS ceramic as a function of Fe_2O_3 doping between 0 and 1.0 wt% were measured at temperature of 300 K, using a maximum magnetic field of 1.0 T (10,000 Oe), and are shown Fig. 25. The undoped KNLNTS ceramic showed the linearization of the M-H curve with a negative slope indicating diamagnetic behavior. When Fe_2O_3 doping increased from 0.2 to 0.4 wt%, the M-H loops were still linear but the slope became more positive, demonstrating that the diamagnetic behavior gradually changed to paramagnetism. The sample with Fe_2O_3 doping of 0.6 wt% presented ferromagnetic behavior with a remnant magnetization (M_r) of 0.015 emu/g and a coercive field (H_c) of 143 Oe, which indicated the increment of ferromagnetic long-range ordering in this sample. When the amount of Fe_2O_3 was between 0.8 and 1.0 wt%, the M-H curves of the samples became close to linear, which was the characteristic of paramagnetic behavior again. The change in magnetic behavior of the transition metal doped ceramic oxides

depending on the doping concentration is quite common [44, 45] via oxygen vacancy in antiferromagnetic materials or to the bound magnetic polaron [46, 47]. The actual underlying reason depends on the charge states and the distribution of the Fe ions. At the moment, it is really difficult to pinpoint the source of the induced ferromagnetism in the KNLNTS sample with 0.6 wt% Fe_2O_3. For in depth explanation, other techniques to verify the charge state of Fe ions and distribution may be required.

Nevertheless, it should be noted that this work is the first to reveal the optimum amount of Fe_2O_3 doping to induce ferromagnetic properties in KNLNTS ceramics. Moreover, it is important to realize that the Fe_2O_3 doping of 0.6 wt% is the optimized amount not only for maximizing ferromagnetic properties but also dielectric, ferroelectric and piezoelectric properties in the KNLNTS ceramics. With a combination of multi-functionalities, the 0.6 wt% Fe_2O_3 ceramic could find many potential applications in spintronics, energy harvesting, or sensors, further investigations of this materials are of interest.

CHAPTER V

CONCLUSION

The KNLNTS lead-free piezoelectric ceramics with Fe_2O_3 doping (0-1.0 wt%) were prepared by the solid state combustion technique. The influence of Fe_2O_3 doping on the phase formation, microstructure, density, electrical and magnetic properties were investigated. The phase formation changed from orthogonal phase to dominate orthorhombic phase and cubic phase when Fe_2O_3 doping increased from 0 to 1.0 wt%. Dopant of Fe_2O_3 between 0.2-0.6 wt% improved the densification and microstructure, which could promote atomic diffusion during sintering by the increase of oxygen vacancies, which were generated by the substitution of Fe^{3+} at the B-site. The optimum condition was obtained by the sample at Fe_2O_3 doping of 0.6 wt% which exhibited the highest density (96.1%), the highest dielectric constant (ε_r=2782 and ε_m=7520), excellent ferroelectric properties (P_r= 27.9 $\mu C/cm^2$ and E_c = 9.9 kV/cm), the maximum d_{33} value (311 pC/N) and induced ferromagnetic properties (M_r = 0.015 emu/g and H_c =143 Oe). In summary, this paper provides a new way to modify densification, morphology, electrical and magnetic behavior of KNLNST lead-free materials.

References

[1] R.E. Jaeger, L. Egerton, J. Am. Ceram. Soc. 45 (1962) 209-213.

[2] M.D. Maeder, D. Damjanovic, N. Setter, J. Electroceram. 13 (2004) 385–392.

[3] Y. Guo, K. Kakimoto, H. Ohsato, Appl. Phys. Lett. 85 (2004) 4121-4123.

[4] H. Takao, Y. Saito, Y. Aoki, K. Horibuchi, J. Am. Ceram. Soc. 89 (2006) 1951-1956.

[5] E. Hollenstein, M. Davis, D. Damjanovic, N. Setter, Appl. Phys. Lett. 87 (2005) 182905-182910.

[6] J. Wu, Y. Wang, D. Xiao, J. Zhu, P. Yu, L. Wu, W. Wu, Jpn. J. Appl. Phys. 46 (2007) 7375-7377.

[7] H.L. Dua, F.S. Tang, D.J. Liu, Mater. Sci. Eng. B 136 (2007) 165-169.

[8] L. Ramajo, R. Parra, M.A. Ramirez, M.S. Castro, Bull. Mater. Sci. 34 (2011) 1213-1217.

[9] M. Kosec, V. Bobnar, M. Hrovat, J. Bernard, B. Malic, J. Holc, J. Mater. Res. 19 (2004) 1849-1854.

[10] Y. Guo, K. Kakimoto, H. Ohsato, Mater. Lett. 59 (2005) 241-244.

[11] Z. Yang, Y. Chang, B. Liu, L. Wei, Mater. Sci. Eng. A 432 (2006) 292-298.

[12] M. Jiang, X. Liu, C. Liu, Mater. Res. Bull. 45 (2010) 220-22.

[13] N.M. Hagh, B. Jadidian, A. Safari, J. Electroceram. 18 (2007) 339-346.

[14] Y. Saito, H. Takao, T. Tani, T. Nonoyama, K. Takatori, T. Homma, T. Nagaya, M. Nakamura, Nature 432 (2004) 84-87.

[15] H.N. Ji, Y.P. Ok, W.P. Tai, J. Korea. Phys. Soc. 56 (2010) 1156-1159.

[16] R. Zuo, Z. Xu, L. Li, J. Phys. Chem. Sol. 69 (2008) 1728-1732.

[17] Y.P. Ok, H.N. Ji, K.S. Kim, W.P. Tai, J.H. Seola, I.K. Hong, J.S. Lee, Mater. Sci. Eng. 18 (2011) doi:10.1088/1757-899X/18/9/092053

[18] Z. Guo, L. Pan, C. Bi, H. Qiu, X.Zhao, L.Yang, M.Y. Rafique, J. Magn. Magn. Mater. 325 (2013) 24-28.

[19] C. Ang, Z. Yu, Z. Jing, P. Lunkenheimer, A. Loidl, Phys. Rev. B 61, 3922-3926.

[20] Y. Yang, C.S. Lin, J.F. Chen, L. Hu, W.D. Cheng, J. Appl. Phys. 116 (2014)153709-15370913.

[20] Y. Yang, C.S. Lin, J.F. Chen, L. Hu, W.D. Cheng, J. Appl. Phys. 116 (2014)153709-15370913.

[21] C.C. Hwang, T.Y. Wu, J. Wan, J.S. Tsai, Mater. Sci. Eng. B 111 (2004) 49-56.

[22] C. Wattanawikkam, N. Vittayakorn, T. Bongkarn, Ceram. Inter. 39 (2013) 399-403.

[23] P. Bhupaijit, C. Kornphom, N. Vittayakorn, T. Bongkarn, Ceram. Int. 41(2015) 81-86.

[24] C. Kornphom, N. Vittayakorn, T. Bongkarn, Ferroelectrics. 491 (2016) 44-53.

[25] C. Kornphom, A. Laowanidwatana, T. Bongkarn, Ceram. Int. 39 (2013) 421-426.

[26] S. Yotthuan, C.Kornphom, T. Bongkarn, Phase Transitions (2015) http://dx.doi.org/10.1080/01411594.2015.1010202.

[27] P. Thawong, C. Kornphom, S. Chootin, T. Bongkarn, Phase Transitions (2015) http://dx.doi.org/10.1080/01411594.2015.1071369

[28]. S.S. Manoharan, K.C. Patil, J Am Ceram Soc. 751 (1992) 1012-1015.

[29] Powder Diffraction File No. 71-0945, International Centre for Diffraction Data, Newton Square, PA, 2000.

[30] Powder Diffraction File No. 71-2127, International Centre for Diffraction Data, Newton Square, PA, 2000.

[31] Powder Diffraction File No. 08-0212, International Centre for Diffraction Data, Newton Square, PA, 2000.

[32] X. Shang, J. Guo, W. Xiao, Y. Lu, G. Chang, T. Zhou, Y He, J. Electron. Mater. 43 [5] (2014) 1424–31.

[33] A. Watcharapasorn, S. Jiansirisomboon, T. Tunkasiri, Mater. Lett. 61 (2007) 2986-2989.

[34] C.X. Li, B. Yang, S.T. Zhang, R. Zhang, Y. Sun, J.J. Wang, R.X. Wang, W.W. Cao, Ceram. Int. 39 (2013) 8701-8708.

[35] Y. Hou, C. Wang, J. Zhao, H. Ge, M. Zhu, H. Yan, Mater. Chem. Phys. 134 (2012) 518- 522.

[36] D. Lin, K.W. Kwok, K.H. Lam, H.L.W. Chan, J. Appl. Phys. 111 (2014) 074111.

[37] Y. Guo, K. Kakimoto, H. Ohsato, Appl. Phys. Lett. 85 (2004) 4121-4123.

[38] M. Matsubara, K. Kikuta, S. Hirano, J. Appl. Phys. 97 (2005) 114105.

[39] M. Matsubara, T. Yamaguchi, W. Sakamoto, K. Kikuta, T. Yogo, S. Hirano, J. Am. Ceram. Soc. 88 (2005) 1190-1196.

[40] X. Shang, J. Guo,W. Xiao, Y. Lu, G. Chang, T. Zhou, Y. He, J. Electron. Mater. 43 (2014) 1424-1431.

[41] C. Kornphom, T. Bongkarn, Mater. Sci. 20 (2014) 479-484.

[42] P.A. Jha, A.K. Jha, J. Alloys Comp. 513 (2012) 580-585.

[43] W. Yansen, D. Kim, K.J. Parwanta, C. Liu, B.W. Lee, Curr. Appl. Phys. 15 (2015) 120-123.

[44] S. Phokha, D. Prabhakaran, A. Boothroyd, S. Pinitsoontorn, S. Maensiri, Microelectron. Eng. 126 (2014) 93-98.

[45] S. Phokha, S. Hunpratup, S. Pinitsoontorn, B. Putasaeng, S. Rujirawat, S. Maensiri, Mater. Res. Bull. 67 (2015) 118-125.

[46] Q. -Y. Wen, H. -W. Zhang, Y. -Q. Song, Q. -H. Yang, H. Zhu, J. Q. Xiao, J. Phys. Cond. Matt. 19 (2007) 246205.

[47] P. A. Wolff, R. N. Bhatt, A. C. Durst, J. Appl. Phys. 79 (1996) 5196.

[48] Jaffe, B., Cook, W.R. and Jaffe, H. (1971). **Piezoelectric ceramics**. India: Ceramic Book and Literature Service.

[49] Azad, A.M., Subrmaniam, S. and Dung, T.W. (2002). On the development of high density barium metazirconate ($BaZrO_3$) ceramics. **Journal of American Ceramics Society,** 334, 118-130.

[50] Sin, A., Montaser, B. El., Odier, P. and Weiss, F. (2002). Synthesis and sintering of large batches of barium zirconate nanopowders. **Journal of American Ceramics Society,** 85, 1928-1932.

[51] Ganguli, A.K., Ahmad, T., Vaidya, S. and Ahmed, J. (2008). Microemulsion Route to the synthesis of nanoparticles. **Pure and Applied Chemistry,** 80, 2451-2477.

[52] Guillaume, B., Boschini, F., Garcia-Cano, I., Rulmont, A., Cloots, R. and Ausloos, M. (2005). Optimization of $BaZrO_3$ sintering by control of the Initial powder size distribution; a factorial design statistical analysis.

Journal of American Ceramics Society, 25, 3593-3604.

[53] Sawyer, C. B. and Tower, C. H. (1930). Rochelle Salt as a Dielectric. **Physics Review**, 35, 269.

[54] Li, W., Xu, Z., Chu, R., Fu, P. and Zang, G. (2012). Enhanced ferroelectric properties in $(Ba_{1-x}Ca_x)(Ti_{0.94}Sn_{0.06})O_3$ lead-free ceramics. **Journal of European Ceramics Societies,** 32, 517-520.

[55] Kornphom, C., Paowsawat, S. and Bongkarn, T. (2014). Phase formation, Microstructure and electrical properties of KNN-BZT ceramics fabricated via combustion technique. **Ferroelectics,** 458, 127-135.

[56] Azad, A.M. and Subramaniam, S. (2002). Temperature dependence of the dielectric response of $BaZrO_3$ by immittance spectroscopy. **Materials Research Bulletin,** 37, 11-21.

[57] Bhupaijit, P., Kornphom, C., Vittayakorn, N. and Bongkarn, T. (2015) Structural, microstructure and electrical properties of La_2O_3-doped $Bi_{0.5}(Na_{0.68}K_{0.22}Li_{0.1})_{0.5}TiO_3$ lead-free piezoelectric ceramics synthesized by the combustion technique. **Ceramics International,** 41, S81-86.

[58] Yotthuan, S., Kornphom, C. and Bongkarn, T. (2015). The effect of firing conditions on phase formation, microstructure and dielectric properties of BNKTNb-LSb ceramics prepared via the combustion technique. **Phase Transitions,** 88, 1035-1043.

[59] Thawong, P., Kornphom, C., Chootin, S. and Bongkarn, T. (2016). Phase evolution and electrical properties of a new system of (1-x)[BNT-BKT-KNN]-xBCTZ lead-free piezoelectric ceramics synthesized by the solid-state combustion technique. **Phase Transitions,** 89, 232-241.

[60] Hench, L.L. and West, J. (1990). **Principles of Electronic Ceramics Hoboken**. New Jersey: John Wiley & Sons Incorporated.

[61] Haertling, H. (1999). Ferroelectric ceramics: History and Technology. **Journal American Ceramic Societies**, 82, 797.

[62] Moulson, A.J. and Herbert, J.M. (2003). **Electroceramics**. New York: Wiley- Interscience.

[63] Fousek, J. (1995). Joseph Valasek and the Discovery of Ferroelectricity. **Proceeding of the IEEE**, 1.

[64] Jona F. and Shirane, G. (1962). **Ferroelectric crystal.** New York: Pergamum Press.

[65] Megaw, H. (1957). **Ferroelectricity in crystals.** London: Methuen.

[66] Chiang, Y. (1997). **Physical ceramics.** New York: John Wiley & Sons.

[67] Guo, R. (2000). Origin of the high piezoelectric response in $PbZr_{1/x}$ TiO_3. **Physics Review Letters**, 84, 5423.

[68] Ganguli, D. and Chatterjee, M. (1997). **Ceramic powder preparation.** USA: Kluwer Academic Publishers.

[69] Cahu, R.W., Haasen, P. and Kramer, E.J. (1996). **Materials sciences and technology**. Germany: The Federal Republic of Germany.

[70] Pierre, A.C. (1998). **Introduction to so-gel processing.** USA: Kluwer Acadamic Publishers.

[71] Ring, T.A. (1996). **Fundamentals of ceramics powder processing and synthesis**. New York: Acdemic Press Inc.

[72] Sumang, R., Wicheanrat, C., Bongkarn, T. and Maensiri, S. (2015). High densification and dielectric properties of lead-free $(K_{0.5}Na_{0.5})NbO_3$ piezoelectric ceramics with optimum excess Na_2O and K_2O contents. **Ceramics International,** 41, S136-S142.

[73] Zuo, R., Fang, X. and Ye, C. (2007). Phase structures and electric properties of new lead $(Na_{0.5}K_{0.5})NbO_3$-$(Bi_{0.5}Na_{0.5})TiO_3$ ceramics. **Applied Physics Letter,** 90, 092904.

[74] Saito, Y., Takao, H., Tani, T., Nonoyama,T., Takatori, K., Homma,T., Nagaya, T. and Nakamura, M. (2004). Lead-free piezoceramics. **Nature,** 432, 84-87.

[75] Jiang, M., Liu, X. and Liu, C. (2010). Effect of $BiFeO_3$ additions on the dielectric

and piezoelectric properties of $(K_{0.44}Na_{0.52}Li_{0.04})(Nb_{0.84}Ta_{0.1}Sb_{0.06})O_3$ ceramics. **Materials Research Bulletin,** 45, 220-223.

[76] Hagh, N.M., Jadidian, B. and Safari, A. (2007). Property-processing relationship in lead-free (K, Na, Li) NbO_3-solid solution system. **Journal of Electroceramics,** 18, 339-346.

[77] Suranarayana, C. and Grant Norton, M. (1998). **X-ray diffraction a practical approach**. New York: Plenum.

[78] Swartz, S.L. and Shrout, T.R. (1982). Fabrication of perovskite lead magnesium niobate. **Materials Research Bulletin,** 17(10), 1245-1250.

[79] **Science Lab Center**. (2004). Retrieved February 1, 2014, from http://www.sci.nu.ac.th/slcs/index.php.

[80] Ronald, E.L. (2010). **Characteization of ceramics**. New York: Momentum.